THE DOE2000 MATERIALS MICROCHARACTERIZATION COLLABORATORY*

E. Voelkl[1], K. B. Alexander[1], J. C. Mabon[2], M. A. O'Keefe[3], M. T. Postek[4], M. C. Wright[5], and N. J. Zaluzec

[1]Metals and Ceramics Division
[5]Instruments and Controls Division
Oak Ridge National Laboratory
Oak Ridge, TN 37831

[2]Materials Research Laboratory
University of Illinois
Urbana-Champaign

[3]National Center for Electron Microscopy
University of California
LBNL B72
Berkeley, CA 94720

[4]Precision Engineering Division
National Institute of Standards and Technology
Gaithersburg, MD 20899

[6]Materials Science Division
Argonne National Laboratory
Argonne, IL 60439

April 1998

Paper submitted to the 14th International Congress on Electron Microscopy, Cancun, Mexico, August 31 - September 4, 1998.

*Work supported in part by the U. S. Department of Energy, BES-Materials Sciences, under Contract W-31-109-ENG-38.

DISCLAIMER

Nomenclature

c_p	specific heat, J/kg.K
D	inner diameter of tube, m
d	pore size, m
d_f	fiber diameter, m
f	friction coefficient
G	mass flow reate, *kg/min*
h	heat transfer coefficient, W/m^2K
k	thermal conductivity, w/m^2K
LN2	Liquid nitrogen
l	length of a tube, *m*
Nu	Nusselt number
p	pressure, Pa
Pe	Peclet number
q''_w	wall heat flux, w/m^2K
Re	Reynolds number
t	time, *sec*
T	temperature, ^oC
u	superficial velocity, m/s
u_o	superficial porous core velocity, m/s

Greek letters

ε	porosity

Subscripts

eff	effective
f	fluid phase
i	inlet
l	saturated liquid
m	mean (bulk)
s	solid phase
sat	saturation
w	inner wall

Introduction

Porous inserts have been used for enhancing heat transfer in cooling channels for high heat flux applications [1-6]. At the Advanced Photon Source facility (APS) at Argonne National Laboratory (ANL), the heat flux from the powerful APS x-ray beam that impinges upon the x-ray beamline components is of the order of 600 W/mm^2 in normal incidence. Through innovative grazing-angle engineering, the actual heat flux impinging on the beam-interacting components is reduced to under 30 W/mm^2, which is manageable using high temperature materials and advanced cooling concepts. Deionized water in single phase is normally used as the cooling medium for beamline components. Safety requires strict equipment and personnel protection system interlocking. Interlocked flow/pressure set points are carefully chosen so as to compromise the high reliability and availability of this complex user facility, which normally operates around the clock. Therefore, two-phase cooling is avoided for assured reliability and mitigation of vibrations. The high heat flux and heat load levels handled by the x-ray components require highly enhanced cooling methods wherever appropriate to assure long-term structural integrity of the components as well as to minimize the use of expensive deionized cooling water in the facility. For high heat transfer enhancement, we have chosen the use of rolled and compressed copper mesh inserts in the cooling channels of a variety of components [7-8]. Extensive research to optimize the cooling enhancement, and to minimize the pressure drop and deionized water use resulted in the selection of an enhanced heat transfer coefficient of the order of 2.5 to 3.0 W/cm^2K. Compared to plain channels of the same size, this enhancement represent, on an average, a 6-7 fold increase in the value of the heat transfer coefficient, while there is similar level of reduction in the required deionized water usage. Figure 1 shows a typical use of the porous copper inserts at the APS. Shown is a photon shutter blade. The photon shutter is used to stop the x-ray beam on demand by the beamline user. In this case the five central channels, which cover the area on which the beam can impinge, are equipped with porous copper inserts that are subsequently brazed to the channel walls for intimate thermal contact. The two side channels are used as inlets for the

deionized cooling water, which returns through the five central channels in parallel flow. Due to the high pressure drop caused by the porous inserts, typical parallel channel flow instability concerns are totally eliminated.

While the enhanced cooling of the mechanical components on the beamlines is satisfied with the above scheme, it has been discovered that cryogenic cooling of the optical components with similar conductive mesh inserts also offers distinct advantages [9-10]. Because the optical components exhibit very low tolerance to flow-induced vibrations and jitter, the use of porous media in the flow channels of such optical elements was suggested. The low flows sufficient for an efficient porous media heat transfer operation, coupled with the intrinsic turbulence-reducing characteristics of such media, achieve highly quiet but very effective cooling in these components. Optical components, exemplified by the monochromator crystals and mirrors, typically use materials such as single-crystal silicon or diamonds, natural or man-made, and specialty ceramics and semiconductors. It is widely known that silicon and especially diamond exhibit very desirable thermo-physical properties at cryogenic temperatures, particularly with liquid nitrogen (LN2). At cryogenic temperatures, the inherent high thermal conductivity of the optical materials as well as the low thermal expansion coefficient (nearly zero for diamond) result in very low thermal distortions in the components, which is very desirable for optical performance [11-13]. In cooling of optical components in high heat flux applications, liquid nitrogen, as a coolant, is an attractive economic choice. On the negative side, cryogenics, in general, will reach boiling at a lower heat flux. They exhibit an undesirable rapid and uncontrollable vapor blanketing upon boiling due to small saturation temperature differences. Porous inserts are known to offset some of the negative aspects of two-phase heat transfer in cryogenically cooled plain-tube channels. The inserts are known to cause larger saturation temperature differences in the cooled channel hence boiling is harder to start in a channel with a porous insert. On the other hand, the bulk temperature difference in the fluid cross section is smaller in a porous medium particularly for metallic inserts, compared to a plain channel. Hence while the

cryogenically cooled plain channels can operate in a subcooled boiling mode, the porous-insert channels are known to transform rapidly from onset of boiling (OOB) to rapid full voiding. Hence the classic onset of nucleate boiling (ONB) followed by a steady nucleate boiling does not generally exist in channels with porous inserts. As such, in the case of porous-channel heat transfer phenomena, we will use the terminology OOB throughout in place of the conventional ONB. Only if acoustically benign and maintainable in a steady fashion subcooled convective boiling permissible is in operations. Otherwise, single-phase cryogenic cooling is the preferred method. Thus one needs to know precisely the initiation of boiling and transition through the subcooled boiling with liquid nitrogen.

The limits of subcooled nucleate boiling in porous media are quite complicated for any modeling or extraction from existing boiling heat transfer correlations. In addition to the complex structure of the medium, sufficient theory is not available to describe a number of the physical aspects of the problem. For instance, what are the criteria for bubble formation? What controls the bubble size and whether it will collapse, stick to the surface or the fibers, or whether it will detach from the surface and move? How much superheat is needed locally for the onset of nucleate boiling? Moreover, nucleation is a statistical process, and the complex structure of the porous matrix makes the problem even more complicated. Due to a lack of theories to characterize these processes on a macroscopic scale, theoretical analysis by numerical simulation seems to be unattainable at this time. Therefore an experimental program was undertaken to generate information that can be used in practice to estimate heat transfer and to predict pressure drop.

Experimental Program

The test tubes, schematically shown in Fig. 2, are made of oxygen-free high conductivity (OFHC) copper. All test tubes are the same size with 12.7-mm (1/2 -in) OD and 9.53-mm (3/8-in) ID. Two Kapton-encapsulated thermofoil heaters are continuously wrapped around the tube with about 1.6-mm spacing in between the wraps. Each heater has been

rated at 250 W heating capacity. Miniature copper-constantan thermocouples (TC) with 0.005-mil wire diameters are attached to the copper surface at six locations using an indium-eutectic solder.

Rolled and uniformly compressed copper mesh is used in the flow channel to enhance heat transfer. These copper mesh inserts were made from what is called 8 X 8 sieve (8x8 openings per inch square) with 0.32-mm-diameter wire, woven fabric. After rolling a cut piece of the copper fabric around a 4-40 threaded stainless steel rod, the mesh is uniformly compressed to shape in an in-house designed and automated mesh-making machine. The initial mesh fabric size determines the desired porosity. Practically thousands of such mesh inserts have been made to size to satisfy the needs of the APS project and for use by other high heat load applications. The mesh-making machine can duplicate the desired finished product shape to within a mil (.025 mm). We are able to produce any mesh from a tight 60 percent porosity to the loosest 90 percent porosity in any increment desired. In the extensive tests, porosity was varied from 70 to 90 in increments of two percent, and the mass flow rate was varied in the range zero to 15 kg/min. For better clarity, however, in the summary plot only the test data for porosities from 70 to 90 percent in increments of four percent are shown. At the APS, the high heat flux components use ε= 76 percent porous mesh in the optimized design for single-phase de-ionized water cooling. In the subsequent cryogenic cooling test, three copper mesh porosities at 76, 82 and 88 percent are utilized with two tubes in each case, one with brazed and another with nonbrazed (mechanical wall contact) mesh. In all cases, tubes were attached to the flexible flow lines via synthetic couplings to reduce axial heat losses.

Each test tube is approximately 343 mm in total length; the copper mesh inside is 305mm long. The Ohmic heated length of the tube is 203mm. Therefore an unheated porous flow entry length of about 50.8 mm exists in each test tube followed by the heated section, ending with another unheated porous section, 50.8 mm long. The hydraulic diameter

length (L/Dh) of the test tubes is approximately 32, and the heated length is about 21. The uniform ohmic heat was applied via a 2 kW capacity-regulated DC power supply.

The test section instrumentation includes instruments to measure mixed mean inlet and outlet temperatures and the inlet-to-outlet differential pressure drop; a precision turbine flow meter in water tests (a precision Coriolis-effect mass flow meter was used in cryogenic tests); and the TC instrumentation. Power input was measured using a combination of a precision shunt for current measurement and precision resistors for the voltage measurements. The TCs were usually placed as an averaging group of two at each measurement point. On all the tubes, the three TC groups were placed at 65 mm (2.56-in); 116 mm (4.62-in); and, 167 mm (6.54-in) from the start of the heated section (x=0 position). These axial TC locations correspond to a flow hydraulic length of (from start of the mesh) 12.7, 17.5 and 26.5 diameters, respectively. In most cases, the heat transfer coefficient extracted at the last TC location is regarded as the representative value. The inside wall temperatures needed to calculate the local heat transfer coefficient at the thermocouple locations were obtained in the conventional manner by subtracting the calculated copper wall temperature drop from the measured outer wall temperatures under the applied uniform heat flux.

Experimental Results with Deionized Water

Pressure Drop with Water

Pressure drop data for the 9.5-mm test tubes used in the experiments are shown in Figs. 3 and 4 for the single-phase water flow in dimensional and non-dimensional, forms respectively. Porosities were varied from 70 to 90 in increments of two percent. However for better clarity in Fig. 3, the data in increments of four percent porosity variation are shown against the square of the mass flow rate.

The pressure drop with porous inserts is large and follows the expected linear variation with the mass flow rate squared. As anticipated also, the higher porosities cause less

pressure drop. Pressure drop measurements are done with good accuracy and show excellent repeatability with negligible scatter.

Non-dimensional pressure drop data, shown as friction coefficient versus Reynolds number (Re), are presented in Fig. 4. Data considered in the plot are all taken at a Re number above 10,000 to be sure that fully developed flow conditions are being treated. The complete pressure drop test data for the brazed insert tubes have been correlated well in the following form:

$$f = 19.73\ Re^{-0.23}\ \varepsilon^{-6.29} \qquad (1)$$

This correlation will be revisited later in connection with the cryogenic tests with liquid nitrogen.

Heat Transfer Data with Water

In Fig. 5, the reduced Nusselt (Nu) number is shown versus the Re number for brazed tubes in porosities from 70 to 90 percent in four percent increments. Again, in the experimental program, data was generated in two percent porosity increments and data follow smoothly the trends shown in Fig. 5 in a regular fashion. A Re number range from 3000 to almost 35,000 is attained using the approach velocity and the tube ID. The solid line is the Dittus-Boelter correlation with cross symbols indicating the experimentally established plain tube data. The slight slope change between the Dittus-Boelter correlation and the plain tube data is assumed to be due to the limited length of the experimental tube ($L/D_h \cong 32$). However, for the porous-insert-tubes, this limitation is not significant as the fully developed flow conditions are attained quickly in the tube.

An examination of Fig. 5 indicates that brazed porous insert channels provide excellent enhancement in heat transfer. Unlike ribbed or finned tubes, the heat transfer enhancement with the porous tubes is effective starting at low Re numbers and diminishes only gradually as the Re number increases. Enhancement appears to be a weak function of

porosity in the data range. With 70 percent porosity, enhancement at Re= 10^4 appears to be about six fold.

One experimentally established strong effect is whether or not the copper insert is brazed into the channel walls. In the non-brazed case, the mechanical fit is a sliding fit. Porous inserts are manufactured within a 25-μm tolerance in diameter. A typical performance difference between the brazed and non-brazed insert cases is illustrated in Figs. 6 and 7 for the 76 percent porosity case (in our optimized use, the ε=76 percent). Figure 6 shows that the pressure drop is about the same with both tubes. It was observed that, if a sliding fit is achieved and the brazing is done carefully, pressure drop with the non-brazed tube will only be about a couple percent lower than the brazed ones. Figure 7 is a plot of the "average heat transfer coefficient" in the test tubes. As expected the brazed tube exhibits a superior heat transfer enhancement compared to the non-brazed tube. We find that data is repeatable in other porosities except that with increasing porosity the difference between the two becomes less pronounced. This is also intuitively correct.

A general correlation is offered in Fig. 8 for heat transfer with water for tubes with brazed porous inserts. This correlation applies to all the tubes we tested from 70 to 90 percent porosity. The correlation form is:

$$Nu_D/\varepsilon^{-1.5} = 0.22\ Pe^{0.63} \qquad (2)$$

Goodness of the fit is 93 % RMS which is very satisfactory. This correlation form will be discussed again later in the study when correlation of heat transfer with cryogenically-cooled porous tubes is examined.

Mathematical Model and Analysis of Single-Phase Flow and Heat Transfer in Porous Cooling Channels

Momentum Transport

For the momentum transfer in the rolled and compressed porous matrix under study, the best fit was found to be a formulation by a mix of Brinkman [14] extension and Cai model [15] with three terms expressing different viscous and inertia effects in the porous matrix as compared to in a packed bed.

$$-\frac{dP}{dx} = C_L \frac{\mu u}{d_f^2}\frac{(1-\varepsilon)^2}{\varepsilon^3} + C_T \frac{\rho u^2}{d_f}\frac{(1-\varepsilon)}{\varepsilon^3} - \frac{\mu}{\varepsilon}\frac{1}{r}\frac{d}{dr}\left(r\frac{du}{dr}\right) \qquad (3)$$

Under incompressible and fully developed flow assumptions, the Brinkman extension is expressed by the third term in Eqn. (3) to satisfy the no-slip boundary condition at the wall. The two empirical constants C and C in Eqn (3) were determined from a curve fit to the experimental pressure drop data with the porous matrix in which the working fluid was water [16]. The values of C_L and C_T were found to be 177.181 and 0.403, respectively, for the porous copper matrix with 75 to 85 percent porosity and a mesh size of 8x8x0.32 mm and 8x8x0.20 mm These values were considered to be sufficiently accurate for water, as well as for liquid nitrogen, as the working fluid.

Energy Transport

Energy transfer was modeled based on the assumption of local thermal equilibrium between the solid and fluid phases in the porous matrix, i.e., by a one-equation model. The transient energy equation was written as

$$\left(\varepsilon \rho_f c_{p_f} + (1-\varepsilon)\rho_s c_{p_s}\right)\frac{\partial T}{\partial t} + \rho_f c_{p_f} u\frac{\partial T}{\partial x} = \frac{\partial}{\partial x}\left(k_{eff_x}\frac{\partial T}{\partial x}\right) + \frac{1}{r}\frac{\partial}{\partial r}\left(k_{eff_r} r\frac{\partial T}{\partial r}\right) + \frac{1}{r^2}\frac{\partial}{\partial \theta}\left(k_{eff_\theta}\frac{\partial T}{\partial \theta}\right) \qquad (4)$$

where subscripts f and s denote the fluid and solid phases, respectively. It should be noted that the first term goes to zero at steady state. However, the solution procedure was based on an explicit finite difference numerical scheme, and, therefore, the transient term was kept. The effective thermal conductivity of the porous medium was based on the work of Koh and Fortini [17] and is expressed as

$$\frac{k_{eff_i}}{k_s} = \left(\frac{1-\varepsilon}{1+n\varepsilon^2} \right) \tag{5}$$

where n is a constant whose recommended value for felt metals is 10, and i can be x , or r direction. The boundary conditions for the problem were as follows:

$$\begin{aligned} &\text{at} \quad r = R \quad u = 0 \qquad \text{no-slip boundary conditions} \\ &\text{at} \quad r = 0 \quad u = u_o \end{aligned} \tag{6}$$

where u_o is the core velocity that can be obtained from the quadratic equation, which results when the Brinkman term is dropped from the momentum equation. The boundary conditions for the energy equation include the inlet fluid condition as well as the prescribed wall heat flux condition. These boundary conditions are expressed as:

$$\begin{aligned} &\text{at} \quad x = 0 \quad T = T_{in} && \text{inlet condition} \\ &\text{at} \quad r = 0 \quad \left.\frac{\partial T}{\partial r}\right| = 0 && \text{symmetry condition} \\ &\text{at} \quad r = R \quad q''_w(\theta) = k_{eff} \left.\frac{\partial T}{\partial r}\right|_{r=R} && \text{wall heat flux condition} \end{aligned} \tag{7}$$

Finite difference methods were used in obtaining the solutions for the above equations. Details have been provided previously [16]. Some sample results are presented here to show the success of the analytical predictions with the earlier test data with water as the coolant. In Fig. 9, experimental and numerical results are provided for the friction coefficient for two test tubes. These tubes have brazed copper mesh; the first one having

75 percent porosity and the second 85 percent porosity. Agreement between the numerical prediction and the experimentally established values is very good.

In Fig. 10, the average heat transfer coefficient along the total tube length is shown against the Re number. Both the calculated values and the experimentally determined values are shown for the two test tubes above. Agreement is satisfactory given the uncertainties involved in establishing the average heat transfer coefficient in the experiments and the analytical modeling of the complex problem. Other analytical predictions have been reported in [16].

The above examples show that analytical prediction of the heat transfer problem with water as the coolant was successful. Application of the analytical techniques to predict the heat transfer with liquid nitrogen cooling is to be tried in future studies.

Cryo-Cooling Experiments with Liquid Nitrogen

Test tubes for the cryogenic tests with liquid nitrogen were made and instrumented as were the deionized water test tubes (Fig. 2). The test section is in a vacuum tank that is kept normally at 10^{-2} Torr. The inlet pressure to the liquid nitrogen pump is adjustable up to 1000 kPa. The closed-loop, pressurized subcooled LN2 pumped through the test section returns to the dewar vessel where it circulates through the heat exchanger submerged in a bath of atmospheric LN2. The atmospheric LN2 boils off, removing heat from the pumped liquid, thereby maintaining a constant fluid inlet temperature to the test section of about 80 K. Liquid nitrogen is introduced into the test section with no super-cooling. The head pressure is regulated to be at a preset value between 80 to 85 psig in all experiments. Hence the saturation temperature of LN2 was about 97 K or so, depending on the head pressure. The total heat load applied to the test section was uniformly set at five values: 100, 200, 300, 400 and 500 Watts.

Experiments measured cryogenic heat transfer using LN2 in round copper tubes. All test tubes were placed in a horizontal configuration in this phase of the experiments. Three copper mesh porosities at 76, 82 and 88 percent were utilized with two tubes in each

case, one with brazed and another with non-brazed (mechanical wall contact) mesh. Further details of the test section and the results will be published [18].

Tubes were tested in a progressive fashion from single-phase heat transfer to the onset of boiling and beyond. A sample case of heat transfer data pertaining to the phenomena described above is shown in Fig.11 for a test tube containing 82 percent porous nonbrazed mesh subjected to a 300 W total heat load. The temperature reading indicated by the end thermocouple (Node #3) is shown, on the right vertical scale, against the stepwise reduced mass flow rate in the test section. Starting at about 3.5 kg/min mass flow rate, the flow was reduced and shows single-phase heat transfer until 0.8 kg/min mass flow is reached. At this mass flow point, onset of boiling (OOB) is reached as indicated by a sudden drop in the wall temperature. A narrow temperature plateau is traced with further reduction in the mass flow rate. This is the subcooled/nucleate boiling width that, with the stepwise reduction in the mass flow rate, degenerates into a rapid voiding and hence a wall temperature runaway condition. At this point the experiment is terminated by manually increasing the mass flow rate to save the test section from a potential burnout.

The average heat transfer coefficient at the same node corresponding to the measured temperature is shown in Fig. 11 on the left vertical scale. It should be noted that, during the single-phase heat transfer tests up to the OOB point, all the thermocouple and the flow-meter data are meaningful. Hence the inlet and outlet TCs along with the flow-meter reading provide an independent check on the heat input (enthalpy rise) into the test section. Up to the OOB point, heat transfer calculations are based upon the known power input and the measured inlet temperature of the single-phase LN2. Bulk fluid temperatures and inner wall temperatures at each node are calculated on this basis. Beyond the OOB point, where two-phase LN2 is present, the enthalpy rise of the fluid as determined by the inlet and outlet TCs along with the mass flow-meter reading does not match the heat input into the test section. An independent measure of fluid quality is

required to account for a proper heat balance. Unfortunately, a means of measuring fluid quality was not available for these experiments. Beyond the OOB point, the measured single-phase enthalpy rise along with the inlet temperature is used to determine a conservative estimate of the heat transfer. Without knowledge of the fluid quality, the known power input will lead to erroneous and sometimes negative results for the heat transfer coefficient if used in these calculations. Consequently, although plotted as read, the quantitative data from the test section should be viewed as suspect beyond the OOB point and can be useful only for trend information.

Pressure Drop

Pressure drop data for the 9.5-mm test tubes used in the experiments are shown in Fig. 12 for the single-phase LN2 flow. The pressure drop in the porous tubes correlates with the square of the flow rate, both for the brazed and the non-brazed inserts. However, the pressure drop in the brazed tube, as expected, is always higher than that in the non-brazed tube at the same flow rate.

Non-dimensionalized pressure drop data shown, as friction coefficient versus Reynolds number, are shown in Fig. 13. Both the brazed and non-brazed data have the same slope. The complete pressure drop test data have been correlated as follows:

$$f = C\ 26.8\ Re^{-0.23}\ \varepsilon^{-6.29} \qquad \text{where,} \qquad (8)$$

C= 1.0 for brazed inserts

C= 0.81 for non-brazed inserts

The correlation form is identical to the one used for the water tests. However, the fit coefficient for the cryogenic case appears to be about 20 percent higher for the brazed porous insert cases. We do not have an explanation for this. In the non-brazed tube tests, same heater tube has been used with different porous inserts. The nature of the fit is a "snug fit" in all cases. If other fit quality is used, the correlation may not be as accurate.

Heat Transfer

Heat transfer data have been analyzed separately for the plain tubes and the tubes with porous conductive inserts. The plain tube single-phase heat transfer has been measured against the traditional Sieder-Tate correlation to verify the experimental procedures for a variety of heater powers from 100 to 500 W (Fig. 14). The solid line is the Sieder-Tate heat transfer correlation for circular plain tube. The single phase heat transfer is consistent with this correlation, with the data scatter within ± 5 percent. In Fig. 14, one can follow the progression of the averaged effective heat transfer coefficient, "h_{eff}", on the tube wall. Progression of forced convection up to the ONB point is a classic case as covered in the foregoing. At and after ONB, the reduced mass flow rate enhances the heat transfer rates from the wall under the combination effect of two-phase forced convection. Hence the averaged effective heat transfer coefficient continually rises until such point where attainment of critical heat flux causes a sudden drop in the effective h_{eff}, where tests were immediately terminated to prevent tube burn-out.

Figure 15 presents the onset of boiling data for the cases of the 9.5-mm diameter (3/8 inch) and the 6.4-mm-diameter (1/4 inch) plain tubes. For the 9.5-mm tube, data are shown for all the uniform heat flux test cases at various mass flow rates from less than 0.5 to 5 kg/min Diversion points from the Seider-Tate curve in Fig.14 are taken to be onset of nucleate boiling (ONB) in a plain tube. At the lowest heater power of 100 W, this occurs at about 0.8 kg/min. At the highest heater power test of 500 W it occurs at about 5 kg/min. The plain tube tests with the 9.5 mm tube is tested at 50 W total power increments. Hence the nine data points for the 9.5-mm tubes plotted in Fig. 15 are taken at heater powers from 500 to 100 W at 50 W intervals. Because the exact location of the ONB could not be determined in the tests, correlation was tested for the two ends of the heater length. The two solid lines show the ONB heat flux using the beginning and the end of heated length based on correlations [19 and 20]. Data are bracketed by the resulting correlation band in close agreement in magnitude and trend. At mass flow rates above the

ONB, heat transfer is single-phase convection. Under the ONB flow rate it is two phase. The ONB heat flux indicated in the vertical ordinate is heat flux at the inner tube wall calculated from the measured total heater power applied via the heaters on the outside tube surface.

Some limited heat transfer measurements were also made with a 6-mm-diameter (1/4 inch) diameter test tube (see Fig. 15). The four data points plotted are taken at 400, 300, 200 and 100 W heater power. At 400 W, the onset of boiling occurred at about 1.8 kg/min and at 100 W at 0.5 kg/min mass flow rate of the liquid nitrogen. Again data are bracketed by the ONB correlation curves using the two ends of the heater length.

Focusing on Fig. 15, one can deduce that, to support a wall heat flux level of 0.1 W/mm^2 without boiling, one has to pass more than 6 kg/min LN2 in a 9.5-mm-diameter tube. At somewhat reduced head pressure this is shown to be reduced significantly to about 3 kg/min. for a 6.4 mm tube. Existing plain tube correlations can be used confidently to determine any parameter needed for a given set of conditions.

Heat Transfer in Tubes with Porous Conductive Inserts

For the 9.5-mm-diameter (3/8 inch) tube, three cases of porosity at 76, 82 and 88 percent have been analyzed. Figure 16 is an illustrative composite plot of the nodal temperature against the varying mass flow rate at a particular case of 300 W total heater power. The plain tube nodal temperature has also been added to provide a basis for comparative discussions.

Focusing on the particular case of 76 percent porosity in Fig. 16, one can see that, as the mass flow rate is continuously reduced from 2.6 kg/min the nodal wall temperature steadily increases as expected. At about 0.4 kg/min mass flow rate, a sudden drop in the wall temperature occurs terminating with a couple prominent narrow peaks followed by a very steep runaway temperature condition. The peaks indicate instability caused by the

onset of boiling at this particular node location. The run-away temperature condition is the very rapid voiding condition in the porous tube after the OOB. Compared to the case of the plain tube provided in the plot, there is no prolonged convection and nucleate boiling regime plateau after the OOB. For the case of the tube with 88 percent porous mesh, the phenomenon is similar except that the single OOB peak is well demarcated and the follow-up boiling regime is still short but a little more lingering than for the case of the tube with 76 percent porous mesh. Hence there appears to be some porosity effect on the apparent width of the boiling plateau.

In addition, the effective heat transfer coefficient, h_{eff},, has been plotted against the mass flow rate. To illustrate the behavior, a composite plot is presented in Fig. 17 for the 76, 82 and 88 percent porosity conditions, for the tubes with both the brazed and non-brazed mesh. Also shown in the same plot are the plain tube test data and the classic Sieder-Tate correlation for a plain tube. Data plots are only shown for the 300 W total heater power case, but trends are similar for all the power test cases run. As the mass flow rate of LN2 through the tube is reduced in a continuous manner at the same heater power and pressure, the heat transfer coefficient is reduced commensurate with some form of the Reynolds number dependence. At a certain point, which is approximately 0.6 kg/min mass flow rate for this chosen case, OOB takes place that is signaled by a sharp rise in the value of h_{eff}. However as noted earlier, a boiling instability sets in quickly as demarcated by a sharp dome. Subsequently, upon a little more reduction in the mass flow rate, the critical heat flux condition is reached for these flow conditions where there is a very sudden drop in the value of h_{eff}. This drop corresponds to the runaway wall temperature condition, at which point the test was terminated.

Under the test conditions applied, ONB for the plain tube is seen to take place at about 2.4 kg/min mass flow rate. The critical heat condition is reached near the 0.8 kg/min mass flow rate. At about 0.5 kg/min mass flow wall temperature, the runaway condition is experienced. In the mass flow rate range from 2.4 to 0.8 kg/min, the plain tube is stable in

the convective nuclear boiling regime. This is beneficial if one is interested to stably cool a heated object with LN2.

Both the tubes with brazed and non-brazed porous mesh have superior heat transfer performance in single-phase LN2 cooling relative to that of the plain tube. Again the brazed porous mesh is superior, in all the cases, to the non-brazed porous mesh. To give some quantitative values, let us focus on the 3.0 kg/min LN2 flow in Fig. 18. The plain tube in single-phase seems to yield an h_{eff} of about 2800 $W/m^2 K$. For the tube with the brazed mesh, h_{eff} is in the range 8,000 to 12,000 $W/m^2 K$ for the three porosities tested. For the tube with the nonbrazed mesh this range is lower, about 6000 to 8000 $W/m^2 K$. Relative to a plain tube with boiling the heat transfer enhancement attained with the porous mesh is significant, i.e., up to a 4-fold increase.

Still another observation from Fig. 18 is that while the plot of the data for the tubes with the brazed mesh exhibits wider scatter, the plot of the data for the tubes with the non-brazed porous mesh is relatively smooth at all power levels. This is not unexpected since brazing of a porous mesh inside a tube, no matter how skillfully done, is difficult to control for uniformity especially at the wall interface. Hence an artificial but inevitable near-wall effect is introduced.

Porous Medium Boiling Heat Transfer Correlations

There are no well-established heat transfer correlations for porous medium in the literature. Several tentative heat transfer correlations have been offered in the form of Nusselt vs. Peclet numbers with or without the explicit term involving porosity [21, 22 and 23]. For forms involving an explicit porosity term, Nu and Pe are based on the hydraulic diameter of the flow tube. For non-explicit forms, Nu and Pe are defined by a characteristic pore size. Thus the porosity effect comes is included in the definition of Nu and Pe. Gortyshov and coworkers [21and 22] offered two correlations explicitly involving the porosity effect.

With porous ceramic inserts:

$$Nu_D = 0.325\ Re^{0.65}\ Pr^{0.56}\ \varepsilon^{-5.6} / Pr_w^{0.14}, \qquad (9)$$

and, with metallic foam inserts:

$$Nu_d = 0.606\ Pe^{0.56}\ \varepsilon^{-5.2} \text{ (claimed to be within 12\% error RMS).} \qquad (10)$$

Of these two correlations, the more relevant latter form has been checked with our experimental data. The characteristic pore size was conveniently determined from a consideration of the cross-sectional geometry of the mesh fabric rolled and pressed into the final insert to achieve the desired porosity. Resulting pore dimensions have been indicated in the figures. Repeated data fits strongly suggested that the best fit was obtained in the above form as long as the explicit porosity term was totally omitted. The porosity effect is already folded into the relationship through using characteristic pore size in defining Nu and Re. If, however, the flow tube hydraulic diameter is used instead, then the explicit porosity term as suggested by Gorytshov was needed. The results are shown in Figs. 19 and 20 for the tubes with the non-brazed porous insert using both correlative forms, respectively:

$$Nu_D/\varepsilon^{-1.5} = 0.28\ Pe^{0.63} \qquad \text{and,} \qquad (11)$$

$$Nu_d = 0.135\ Pe^{0.62} \qquad (12)$$

In either form the fit is good within R=97 percent RMS. But the data fit into correlative form is not as successful for the tubes with the brazed inserts. The best fit to the data is represented by:

$$Nu_d = 0.727\ Pe^{0.467}, \qquad (13)$$

with a fit goodness factor of R= 87 percent RMS. The larger deviation to the fit should be expected because of the much larger data scatter in brazed tube tests as opposed to the data with the non-brazed tube. It is suspected that the previously alluded near-wall effects are responsible for the increased data scatter.

Heat Transfer Enhancement Using Porous Mesh

Porous mesh inserts in flow channels result in large heat transfer enhancement, which has been very well established. However in cryogenic applications, as in optical crystal cooling, emphasis has been shifted from enhancement level to maximum practicable flux level such that cryogenic cooling is viable without going into full boiling due to the low heat flux levels associated with cryogenics at the onset of boiling.

An unpublished a literature review [24] revealed a very limited number of investigations that analyzed heat transfer in forced convective boiling flow in tubes/channels with porous inserts of different configurations. In chronological order, these are the investigations reported by Megerlin *et al.* [1], Gortyshov *et al.* [22] and Kuznetsov and Chikov [23]. Megerlin and coworkers investigated single-phase flow as well as forced convective boiling flow heat transfer in stainless steel tubes with stainless steel mesh and brush inserts. In single-phase, they reported heat transfer rates increased up to nine times in convective heat transfer in tubes with mesh inserts as compared to the case of plain tubes. They also reported that the burnout heat fluxes were 2 to 3 times the values for plain tubes for the same mass fluxes. Roizen *et al.* [25] reported work in which the porous inserts were made of highly permeable porous cellular porcelain. They too found that the critical heat fluxes accompanying boiling in a channel with porous inserts was 2.5 to 3 times higher than the values in channels with no inserts for the same mass fluxes. And finally, Kuznetsov and Chikov [23] also stated that " . . . the critical heat flux in a porous channel is several times higher than that in a smooth one when dealing with high velocity flows in short channels." It should be emphasized that no such comparisons are available regarding the onset of subcooled nucleate boiling. Here emphasis is on the ONB

point because, once this is reached, there is a very short operational span before the tube will be substantially voided. Hence, with tubes having porous inserts in forced convection, the farthest point one can comfortably operate is the subcooled nucleate boiling point.

Results from the test data on the OOB point heat flux versus the mass flow rate are plotted in Fig. 20 for all test tubes. Obviously, all the OOB data for the tubes with non-brazed porous inserts are almost independent of porosity. Hence reviewing a case at 1 kg/min mass flow rate, the maximum boiling heat flux is about 0.06 W/mm^2. The OOB for the plain tube occurs at 0.02 W/mm^2. Thus we see a factor of three enhancements in heat transfer over that for a plain tube, in agreement with the conclusion reached by other researchers cited above. A stronger porosity effect was found for the tubes with the brazed porous inserts. Heat transfer enhancement at OOB is certainly larger than 3-fold relative to a plain tube, and, for the tubes with 76% porosity, it is nearly a 4-fold enhancement. The OOB heat flux for the tube with the 76% porous insert is about 0.08 W/mm^2.

A recent study examined a LN2 cooled silicon crystal using our 6.4-mm (0.25-inch) porous copper inserts [26]. Seven such porous inserts mechanically forced into the cooling channels, 60 mm long, were used to cool the crystal during an x-ray beam experiment. The data showed that, by using LN2 flow in the range 10.4 to 13.1 l/min for the crystal, up to 1800 W total power from the x-ray beam could be supported before ONB was detected. (The monochromator absorbed at least 80 percent of the incident power.) The average heat flux on the surface under the beam was as high as 19 W/ mm^2. The input data translate into an average coolant channel wall heat flux of about 1.44 W/mm^2 and a heat transfer coefficient of about 0.26 W/cm^{2}K from the Dittus-Boelter correlation. Obviously, a significant enhancement of the heat transfer coefficient was achieved using the copper porous inserts in the 6.4-mm-diameter channels to support the heat flux levels cited in the study without the OOB. The study concluded that, for the

same flow rate, a cryo-cooled silicon crystal with 76% porous inserts would support a 3-fold higher total heat load compared to a crystal with plain channels before OOB was encountered (1800 W versus 600 W). In an unpublished work [24] based on the existing literature, the authors also pragmatically concluded that, with the 76% porous 9.5-mm channels, an average channel wall heat flux of about 1.42 W/ mm^2 could be supported in the subcooled boiling regime with LN2 at a 13.5 l/min flow rate (9.54 kg/min). For high-precision optical work, this is of course operationally unacceptable because of the inevitable flow jitter at such high flow speeds (2.7 m/s). However, it may be acceptable in applications that are not sensitive to flow-induced vibrations. For enhanced heat transfer with porous inserts in a 9.5-mm-diameter channel, one may suggest a practical operational range of 3.2 to 4.7 kg/min LN2 flow per channel, which should support 0.8 to 1.0 W/ mm^2 coolant wall heat flux without the voiding concerns.

In conclusion, the tubes with non-brazed porous inserts require much higher boiling heat flux relative to a plain tube under the same operational conditions to initiate boiling. Tubes with brazed porous inserts require an even higher, up to 4-fold, increase in heat flux to initiate boiling.

Heat Transfer Enhancement Versus Pressure Drop Considerations

No heat transfer enhancement is complete without discussing the attendant pressure drop considerations, which is addressed in the following. In single-phase water cooling, our engineering applications have been optimized using porous copper mesh with 76% porosity. The typical 9-mm flow channel we use has a rather larger pressure drop, about 7 kPa/cm at about 0.1 kg/s mass flow of deionized water (DIW). This yields significant enhancement of the convective heat transfer coefficient at about 2.8 W/cm^2K. Our optimization has been driven to achieve the required heat transfer enhancement with minimal deionized water use rather than for minimization of the pressure drop (pumping power). Outside this specific choice for our applications, the heat transfer coefficient

versus the pressure drop relationship is presented in Fig.21 for all the test cases in the study with water. Data in Fig.21 suggests that effect of porosity variation in the range from 70 to 90 percent on enhancement of heat transfer is rather limited. In this range, the maximum "Δh" increment achievable appears to be within 500 W/m^2K at all specific pressure drop levels.

In the optical element cooling case using a cryogen like LN2, the inherent poor heat transfer capacity and low boiling heat flux of LN2 are the primary concerns. Again maximum heat transfer enhancement is the prime consideration rather than optimization of the pumping power. Fig. 22 has been plotted with this optimization criterion in mind and shows the heat transfer coefficient versus the pressure drop in a typical 9.5-mm flow channel. First, we observe that, for the same pressure drop, the tubes with brazed porous inserts will have a higher heat transfer coefficient relative to the tubes with non-brazed porous inserts. This difference is as much as 50% if curve fits were passed through the test data, which exhibit sizable scatter particularly with the brazed tubes. The relative increase in the magnitude of the heat transfer coefficient levels off at about the 200 kPa/m pressure drop level. While this level of pressure drop appears to be very large in applications with long cooling channels and almost not sustainable for even subcooled LN2 operations, in real life applications, it is, in fact, very usable. To give an example, in a typical application of optics cooling, a monochromator crystal will be of the order of 15 cm long. To achieve a high effective heat transfer coefficient, say, above 1 W/cm^2 K, the pressure drop through the optics will be of the order of 30 kPa.

Conclusions

Conductive porous inserts in flow channels achieve superior heat transfer enhancement in special applications. We have examined heat transfer with deionized water and liquid nitrogen in tubes that have brazed or non-brazed porous copper matrix inserts with varying porosities. The intent here has been to understand the dynamics of heat transfer

and pressure drop in porous tubes with convective cooling. Pressure drop and heat transfer correlations have been generated for a set of porosity values with a particular tube size of 9.5-mm ID (also 6-mm ID tube in cryogenic studies).

Heat transfer experiments prove that the insertion of porous copper mesh into plain tubes enhances the convective heat transfer coefficient significantly. With water cooling, the enhancement achievable in single-phase heat transfer is virtually unlimited and totally a function of the pressure drop supportable in a particular application. In our particular application, an optimal enhancement level of about 6-7 fold has been achieved while accepting a tolerable pressure drop.

However in the case of cryogenic cooling, the achievable heat transfer enhancement is bound by the onset of boiling (ONB) in porous tubes. Unlike the case of the plain tube, once the boiling is initiated, such tubes tend to void very rapidly with practicably no sustainable margin in the nucleate boiling regime, for example. In boiling, with tubes in which the porous insert is brazed to the tube wall for the best thermal contact, the heat transfer enhancement is found to be of the order of four-fold relative to a plain tube. This is of the same order of magnitude, albeit somewhat higher, that the few studies in this area had shown previously. Certainly this enhancement and the accompanying pressure drop are related to the porosity. While the lower porosity has the highest specific heat transfer enhancement; optimized against the specific pressure drop, the higher porosity tube will give a better heat transfer coefficient enhancement.

The onset of nucleate boiling (ONB) in plain tubes is found to be very predictable with the existing correlations. No such correlations exist for the tubes with porous inserts.

Porous matrix inserts offer a significant advantage in cooling, providing a jitter-free operation and a much higher effective heat transfer coefficient, at grossly reduced flow rates relative to plain tubes and finned tubes. The jitter-free characteristic of fluid flow

with porous insert makes them eminently useful where flow-induced vibration is a concern in the performance of devices such as high-precision optical devices like mirrors and monochromators.

Acknowledgments

Use of the Advanced Photon Source was supported by the U.S. Department of Energy, Basic Energy Sciences, Office of Energy Research, under Contract No. W-31-109-Eng-38.

References:

[1] Megerlin, F. E. Murphy, R.W. and Bergles, A.E., "Augmentation of Heat Transfer in Tubes by Use of Mesh and Brush Inserts," Trans. ASME J. Heat Transfer, Vol.96, pp.145-151, 1974

[2] Apollonov, V.V. et al., Increase in the Thresholds for Optical Failure of Metallic Mirror Surfaces during Cooling through Structure with Open Porosity," Pis'ma Zh. Tekh. Fiz., 4, No.19, pp.1193-2297, 1978

[3] Polyaev, V. M. and Maiorov, V. A.," Heat Exchange in a Channel with Porous Inserts in a Forced Cooling System," Izv. Vyssh. Uchebn. Zaved., Mashinostr., No.7, pp.51-55, 1982

[4] Mairov,V.A. et al., "Intensification of Convective Heat Exchange in Channels with Porous High-Thermal-Conductivity Filler. I. Heat Exchange with Local Thermal Equlibrium inside the Permeable Matrix," Inzhenerno-Fizicheskii Zhurnal, Vol. 47(1), pp.13-24, 1984

[5] Mairov, V.A. et al., "Intensification of Convective Heat Exchange in Channels with Porous High-Thermal-Conductivity Filler. II. Forced Heat Transfer Regime," Inzhenerno-Fizicheskii Zhurnal, Vol. 47(1), pp.199-205, 1984

[6] Apollonov, V.V et al., "Thermophysical Principles of Cooled Laser Optics Based on New-Type Penetrable Structures," Experimental Heat Transfer, Fluid Mechanics and Thermodynamics (Eds. R.K.Shah, E. N. Ganic and K.T.Yang), Elsevier Science Publishing Co., 1988

[7] T. M. Kuzay "Fixed Mask Assembly Research for Advanced Photon Source Insertion Devices," Argonne National Laboratory Report ANL-90/20 (January 1990)

[8] Kuzay, T.M, Collins, J.T, Khounsary, A.M. and Morales Gilberto, "Enhanced Heat Transfer With Wool-Filled Tubes," ASME /JSME 3rd Joint Heat Conference, Book No. I0309E-1991, Reno, Nevada, pp. 145-151, 1991

[9] Process of Making Cryogenically Cooled High Thermal Performance Crystal Optics, U.S. Patent 5,123,982, 1992

[10] T. M. Kuzay, " Cryogenic Cooling of X-ray Crystals Using A Porous Matrix", Rev. Sci. Instrum. 63 (1), 468-472, 1992

[11] Lin Zhang, "Cryogenic Cooled Silicon-Based X-ray Optical Elements- Heat Transfer Limit", SPIE Vol. 1997 High Heat Flux Engineering II, pp. 223-229 (1993)

[12] B. X. Yang et al. " Performance analysis of cryogenic silicon Laue monochromators at APS undulators", SPIE Vol. 1997 High Heat Flux Engineering II, pp. 302-315 (1993)

[13] Z. Wang et al., "Thermal and deformation analysis of a cryogenically cooled silicon monochromator for high-heat-flux synchrotron sources", Rev. Sci. Instrum. Vol. 66 (2), pp. 2267-2269, 1995

[14] Brinkman, H. C., "A Calculation of the Viscous Force Exerted by a Flowing Fluid on a Dense Swarm of Particles", App. Sci. Res., vol. A1, pp. 27-34, 1947

[15] Cai, Z., "Evaluation of the Non-Darcy Flow through Fibrous Media," J. Material Processing and Manufacturing Science, Vol. 2, pp. 19-39, 1993

[16] M. Sözen, T. M. Kuzay, " Enhanced Heat Transfer in Round Tubes with Porous Insert," Int. J. Heat and Fluid Flow, Vol. 17, 124-129, 1996

[17] Koh, J. C. Y. and Fortini, A., "Thermal Conductivity and Electrical Resistivity of Porous Material," Topical Report, NASA CR-120854, 1971

[18] T.M. Kuzay, J.T. Collins and J. Koons, "Boiling Heat Transfer in Channels with Porous Copper Inserts," submitted for publication in Int. J. Heat & Mass Trans.

[19] Van P. Carey, *Liquid-vapor Phase-change Phenomena*, Hemisphere Publishing, 1992, pp.491-506.

[20] Collier, John. G., *Convective Boiling and Condensation*, McGraw Hill, 1972

[21] Yu.F. Gortyshev, G.B.Murav'ev, and I.N.Nadyrov, "Experimental Study of Flow and Heat Exchange in Highly Porous Structures," Engng -Phys. Journal, 53, 357, 1987

[22] Gortyshov, Y. F., Nadyrov, I. N., Ashikmin, S. R. and Kunevich, A. P., "Heat Transfer in the Flow of a Single-Phase and Boiling Coolant in a Channel with a Porous Insert," J. Engineering Physics and Thermophysics (trans. from Russian), vol. 60(2), pp. 202-207, 1991

[23] Kuznetsov, V. V. and Chikov, S. B., "Heat Transfer under Conditions of Flow along a Fuel Element Placed in a Porous Medium," High Temperature (trans. from Russian), vol. 31(2), pp. 242-246, 1993

[24] M. Sözen and T. M. Kuzay, "A study of cryo-cooling of high heat flux components by the use of cooling channels with porous inserts," Unpublished, July 1995.

[25] Roizen, L. I., Rachitskii, D. G., Rubin, I. R., Vertogradskaya, L. M., Yudina, L. A. and Pypkina, M. B., "Heat Transfer with Boiling of Nitrogen and Freon-113 on Porous Metallic Coatings," High Temperature (trans. from Russian) Vol. 20(2), pp. 264-270, 1982

[26] C. S. Rogers, D. M. Mills, and W. -K. Lee, "Performance of a liquid-nitrogen-cooled, thin silicon crystal monochromator on a high-power, focused wigler synchrotron beam", Rev. Sci. Instrum, 66(6), 3494-3499, 1995

Figure Captions:

Figure 1. Use of copper mesh inserts at the Advanced Photyon Source x-ray beam photon shutters. The five central channels have porous copper inserts. The two side channels are inlets for deionized cooling water.

Figure 2. Schematic of the instrumented test tube.

Figure 3. Pressure loss vs. mass flow rate squared for tubes containing mesh inserts of various porosities and with water as the coolant.

Figure 4. Friction factor vs. Reynolds number correlation in tubes with inserts of various porosities and with water as the coolants.

Figure 5. Correlation of Nusselt number versus Reynolds number for tubes containing inserts with various porosities and comparison with the values for plain tubes.

Figure 6. Pressure drop versus mass flow rate for a tube containing either brazed or nonbrazed 76% porous mesh.

Figure 7. Average heat transfer coefficient data vs. mass flow rate for the 9.5-mm-diameter tube containing either brazed or nonbrazed 76% porous mesh.

Figure 8. Heat transfer correlation of Nusselt number with Peclet number in water for tubes containing brazed porous inserts at porosities from 70 to 90 percent.

Figure 9. Analytical prediction of the friction factor versus Reynolds number for two test tubes. Tube 1 has a 75% porosity; tube 2 has an 85% porosity insert. Both inserts are brazed.

Figure 10. Analytical prediction of the average heat transfer coefficient versus Reynolds number for the two test tubes described in Fig. 9.

Figure 11. A sample case of experimental data for the surface temperature and the average heat transfer coefficient. The tube contained 82% nonbrazed porous mesh. The total heat load was 300 W. The right vertical scale indicates the temperature reading measured by the end thermocouple (Node #3).

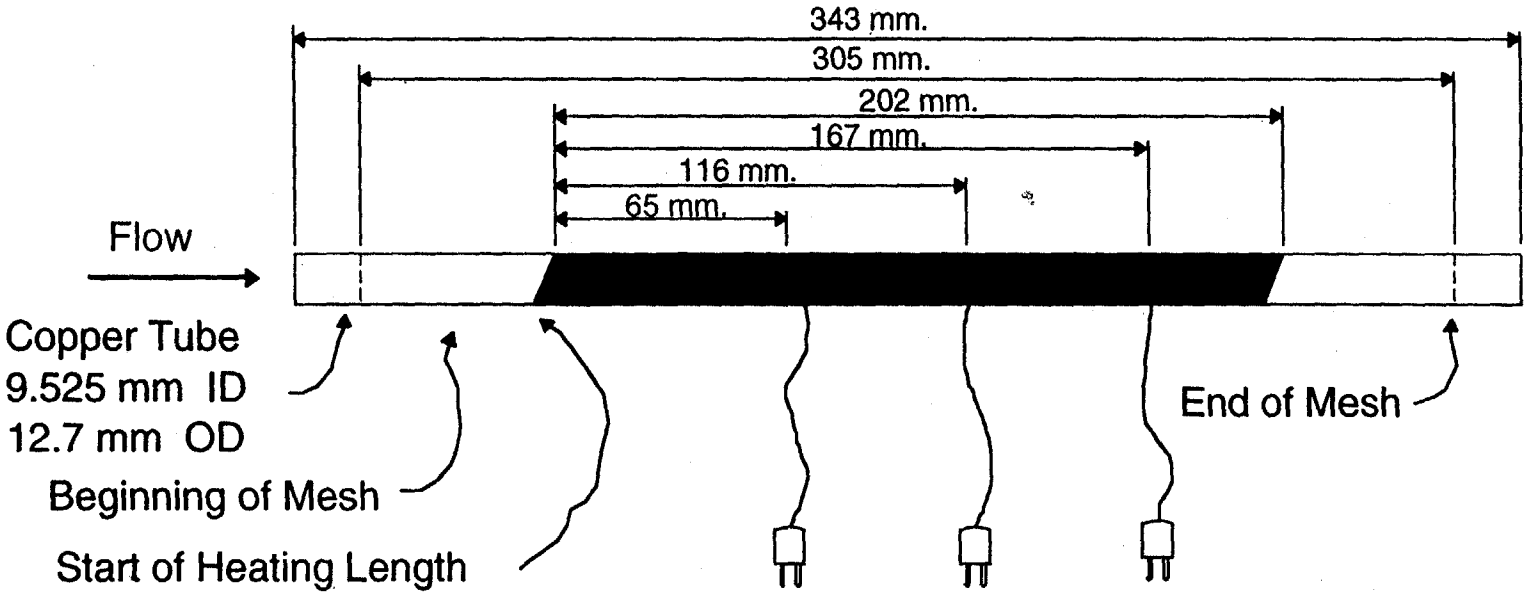
343 mm.
305 mm.
202 mm.
167 mm.
116 mm.
65 mm.
Flow
Copper Tube
9.525 mm ID
12.7 mm OD
Beginning of Mesh
Start of Heating Length
End of Mesh

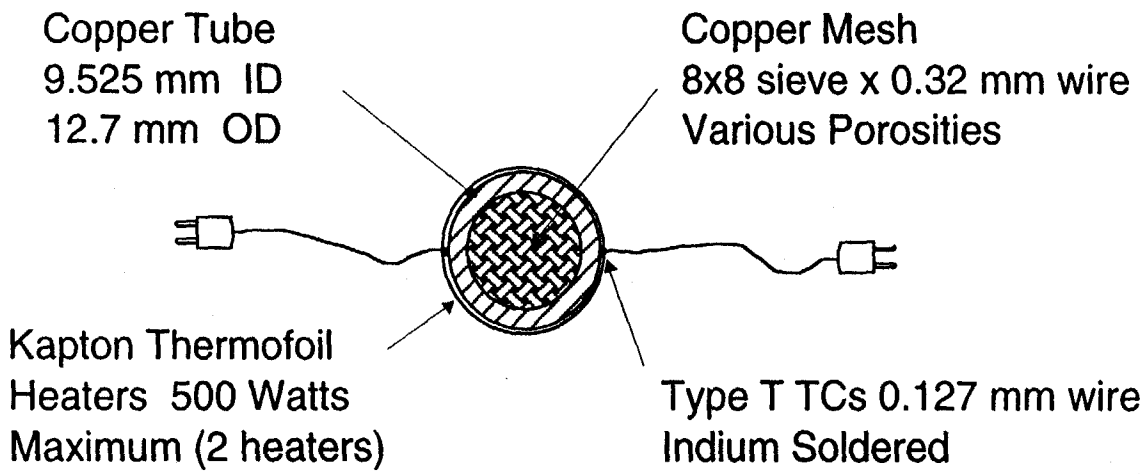
Copper Tube
9.525 mm ID
12.7 mm OD
Copper Mesh
8x8 sieve x 0.32 mm wire
Various Porosities
Kapton Thermofoil
Heaters 500 Watts
Maximum (2 heaters)
Type T TCs 0.127 mm wire
Indium Soldered

Fig. 2

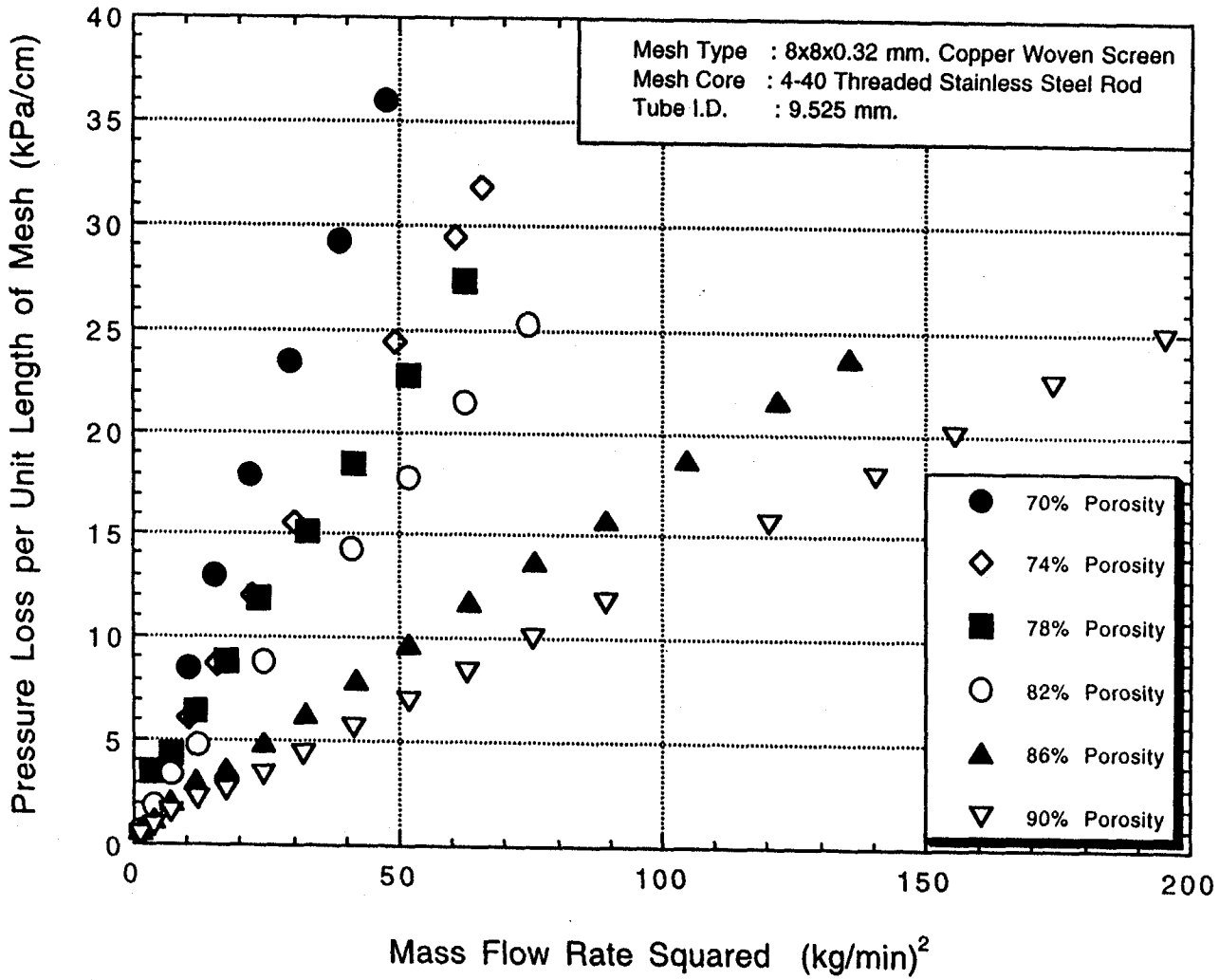
Mesh Type : 8x8x0.32 mm. Copper Woven Screen
Mesh Core : 4-40 Threaded Stainless Steel Rod
Tube I.D. : 9.525 mm.
70% Porosity
74% Porosity
78% Porosity
82% Porosity
86% Porosity
90% Porosity
Pressure Loss per Unit Length of Mesh (kPa/cm)
Mass Flow Rate Squared (kg/min)^2
0
5
10
15
20
25
30
35
40
0
50
100
150
200

Fig. 3

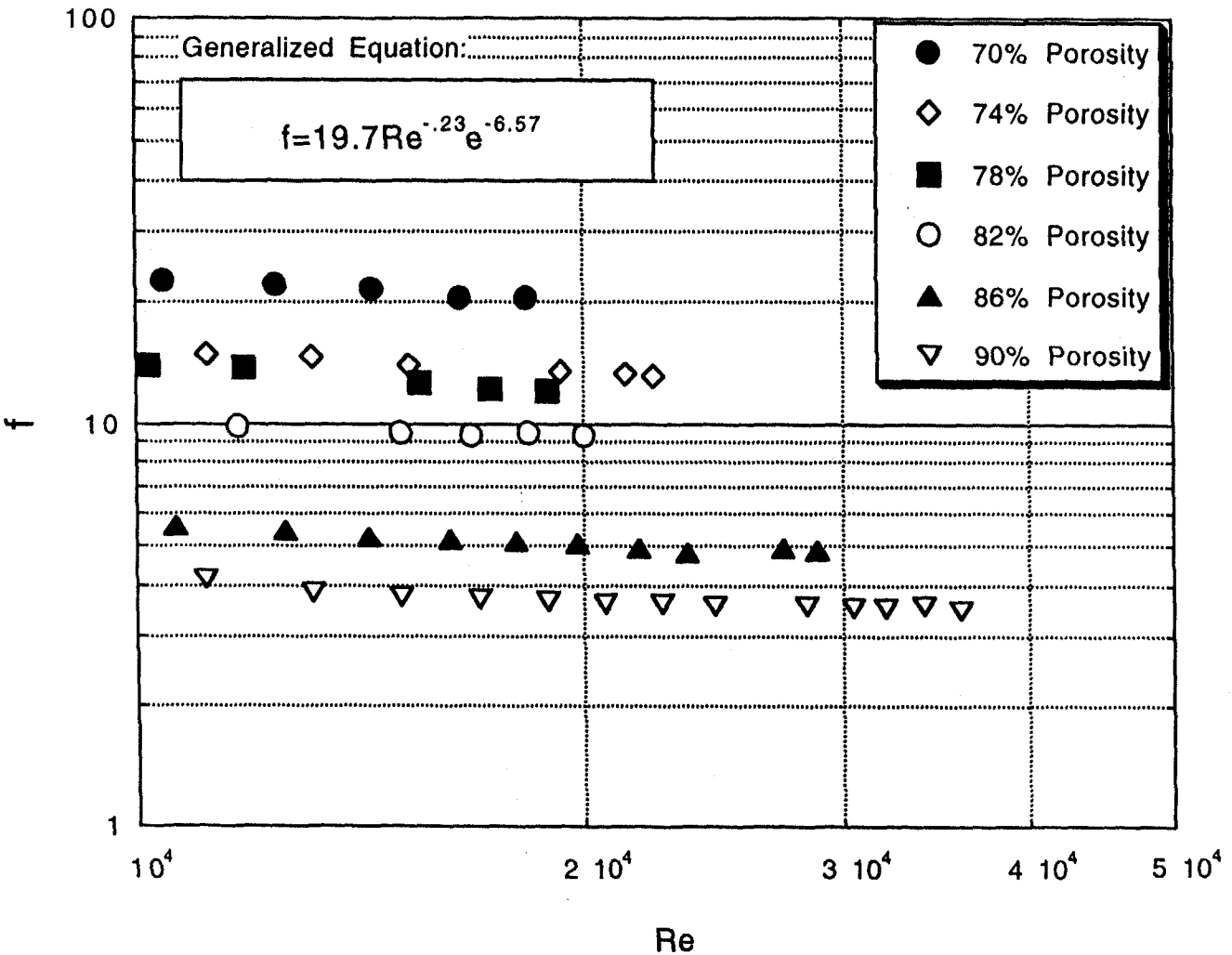
100
10
1
f
Generalized Equation:
f=19.7Re^-.23 e^-6.57
70% Porosity
74% Porosity
78% Porosity
82% Porosity
86% Porosity
90% Porosity
10^4
2 10^4
3 10^4
4 10^4
5 10^4
Re

Fig. 4

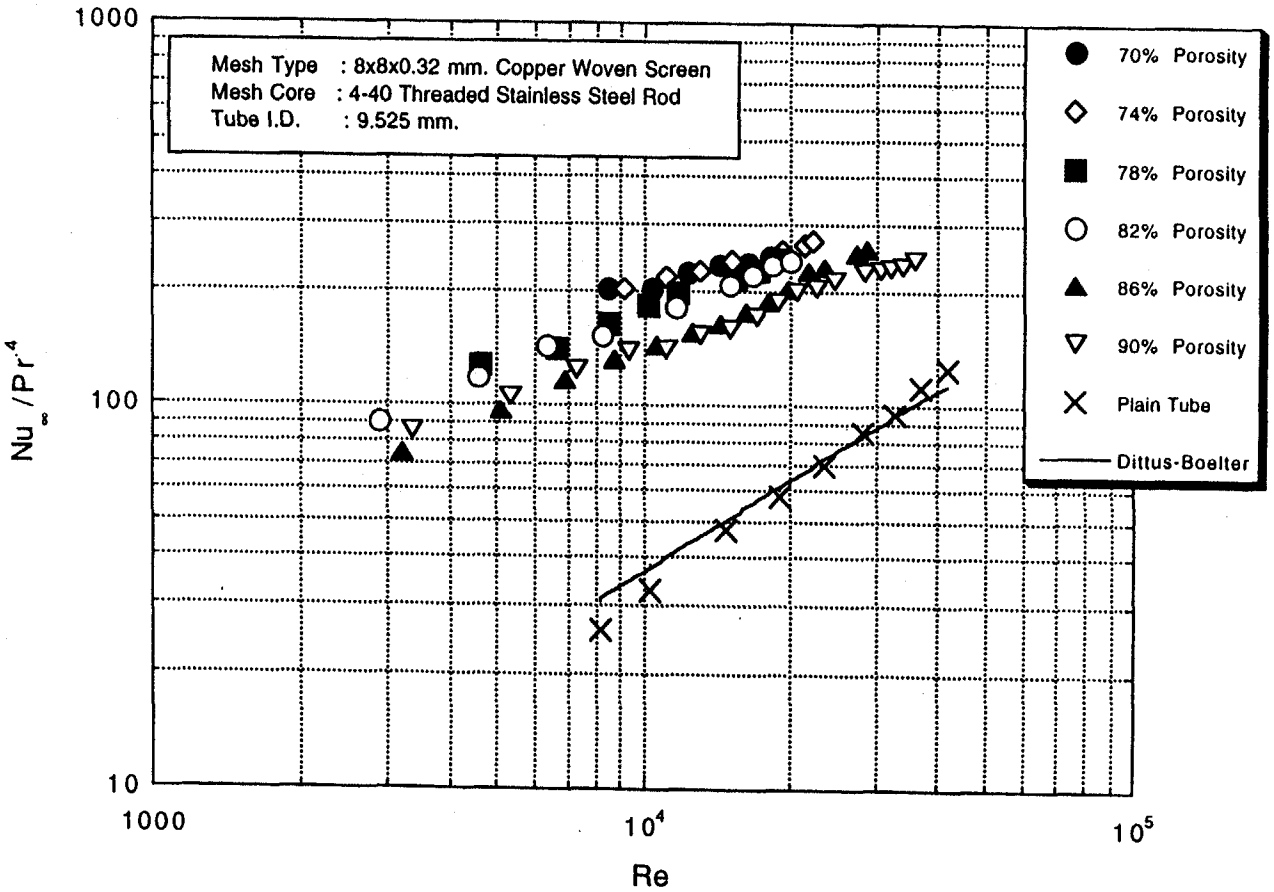
Mesh Type : 8x8x0.32 mm. Copper Woven Screen
Mesh Core : 4-40 Threaded Stainless Steel Rod
Tube I.D. : 9.525 mm.
70% Porosity
74% Porosity
78% Porosity
82% Porosity
86% Porosity
90% Porosity
Plain Tube
Dittus-Boelter
1000
100
10
1000
10^4
10^5
Re
Nu_∞ /Pr^4

Fig. 5

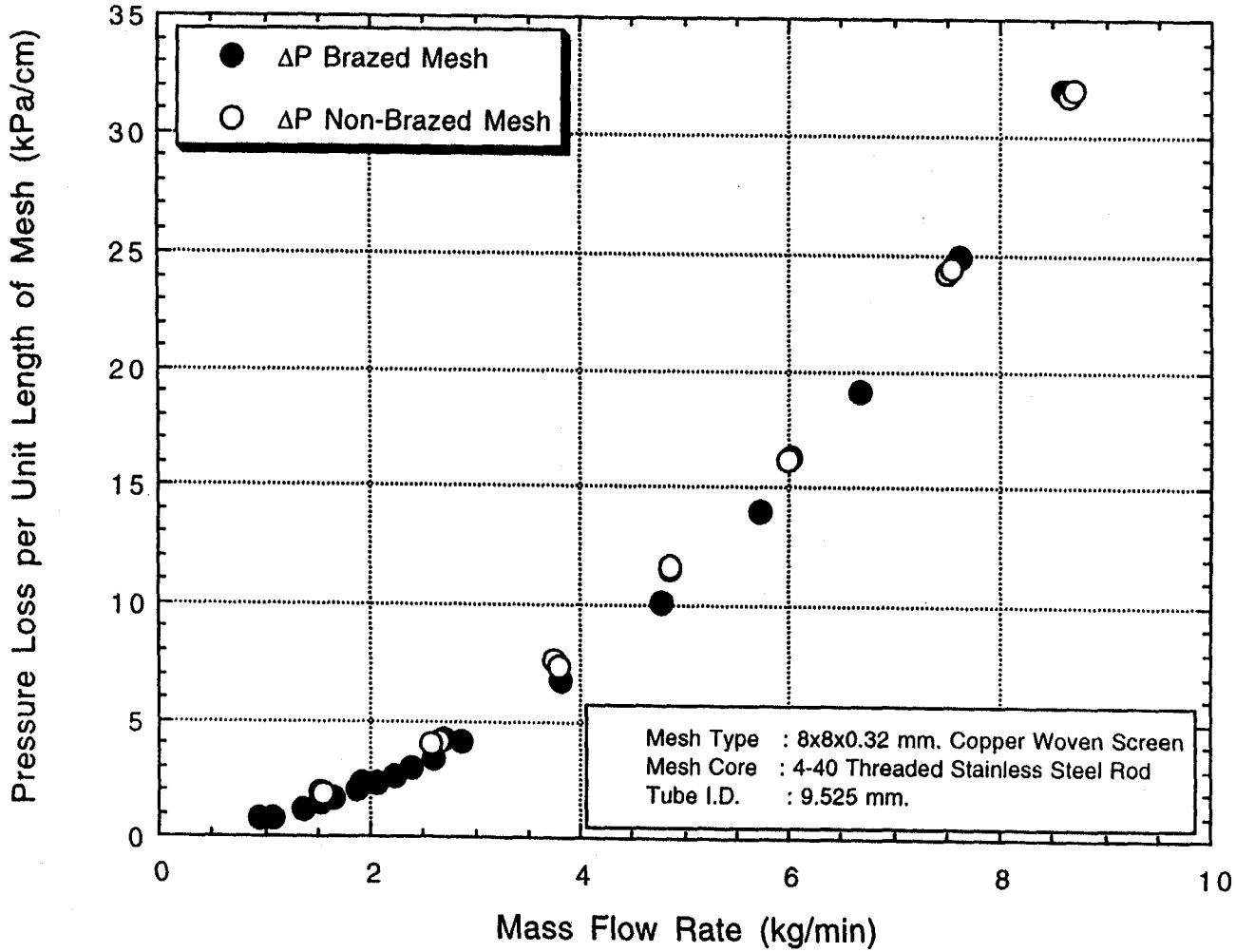
ΔP Brazed Mesh
ΔP Non-Brazed Mesh
Mesh Type : 8x8x0.32 mm. Copper Woven Screen
Mesh Core : 4-40 Threaded Stainless Steel Rod
Tube I.D. : 9.525 mm.
Pressure Loss per Unit Length of Mesh (kPa/cm)
Mass Flow Rate (kg/min)
0
5
10
15
20
25
30
35
0
2
4
6
8
10

Fig. 6

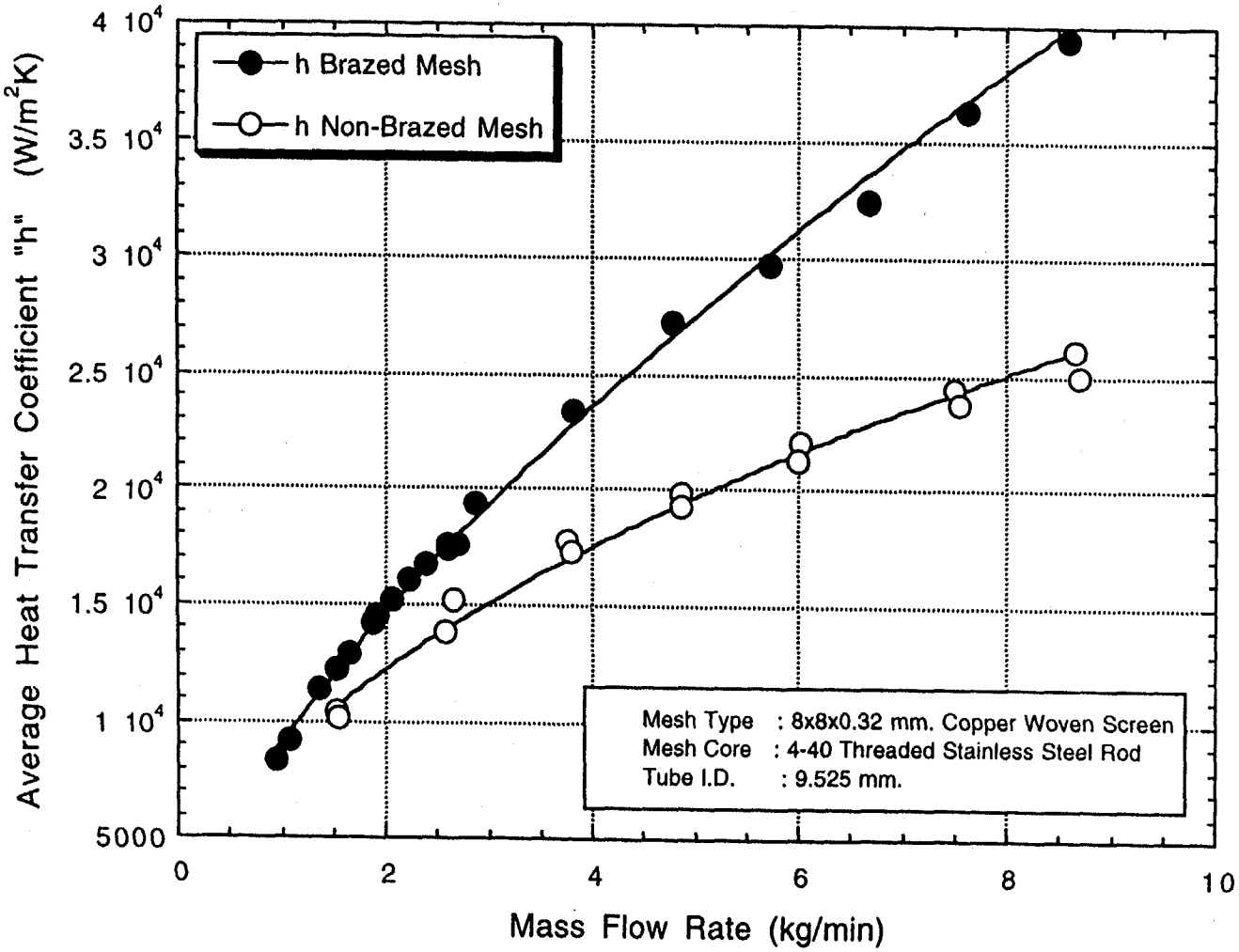
h Brazed Mesh
h Non-Brazed Mesh
Mesh Type : 8x8x0.32 mm. Copper Woven Screen
Mesh Core : 4-40 Threaded Stainless Steel Rod
Tube I.D. : 9.525 mm.
Average Heat Transfer Coefficient "h" (W/m²K)
Mass Flow Rate (kg/min)
4 10⁴
3.5 10⁴
3 10⁴
2.5 10⁴
2 10⁴
1.5 10⁴
1 10⁴
5000
0
2
4
6
8
10

Fig. 7

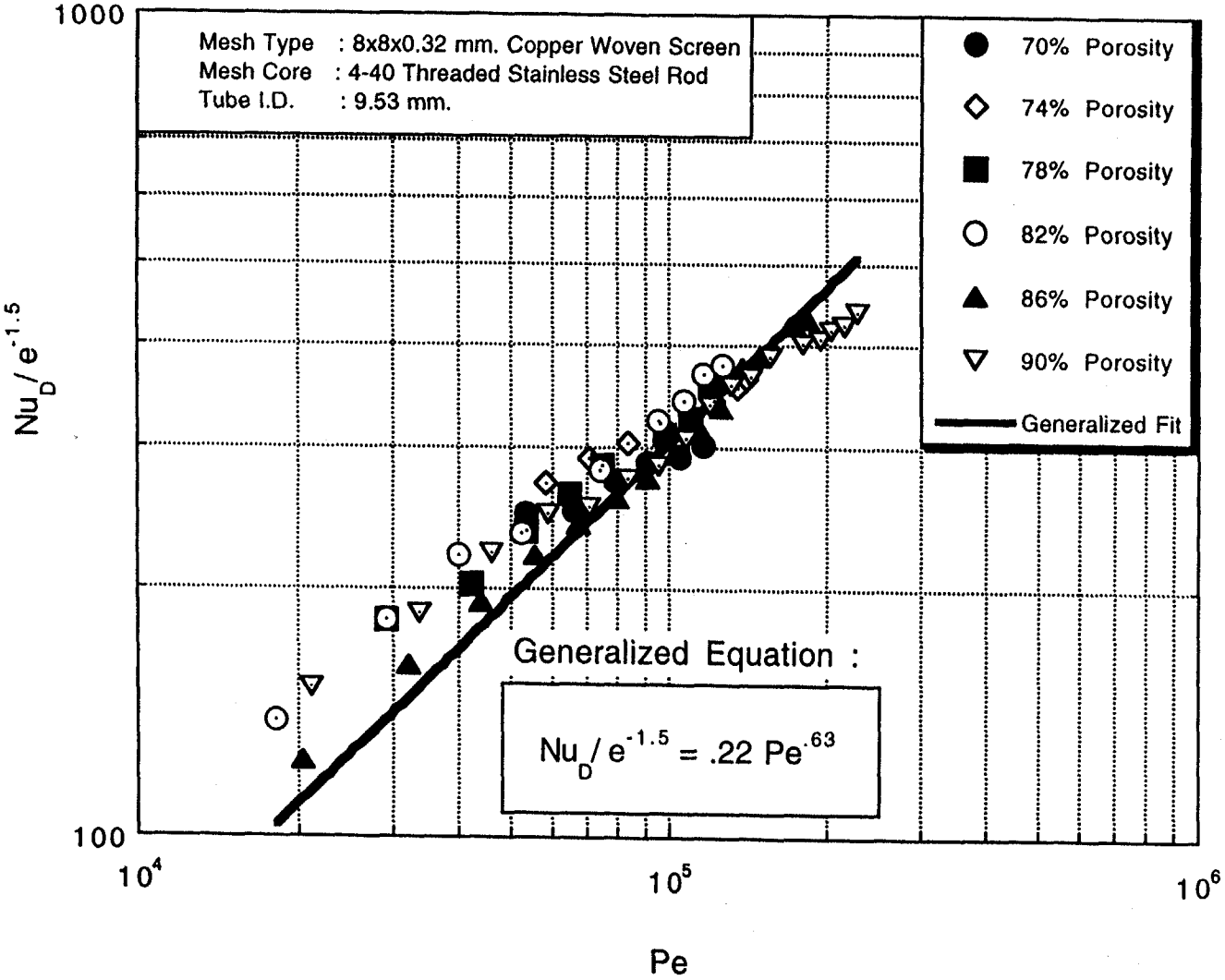
Mesh Type : 8x8x0.32 mm. Copper Woven Screen
Mesh Core : 4-40 Threaded Stainless Steel Rod
Tube I.D. : 9.53 mm.
70% Porosity
74% Porosity
78% Porosity
82% Porosity
86% Porosity
90% Porosity
Generalized Fit
Generalized Equation :
$Nu_D / e^{-1.5} = .22\ Pe^{.63}$
1000
100
10^4
10^5
10^6
$Nu_D / e^{-1.5}$
Pe

Fig. 8

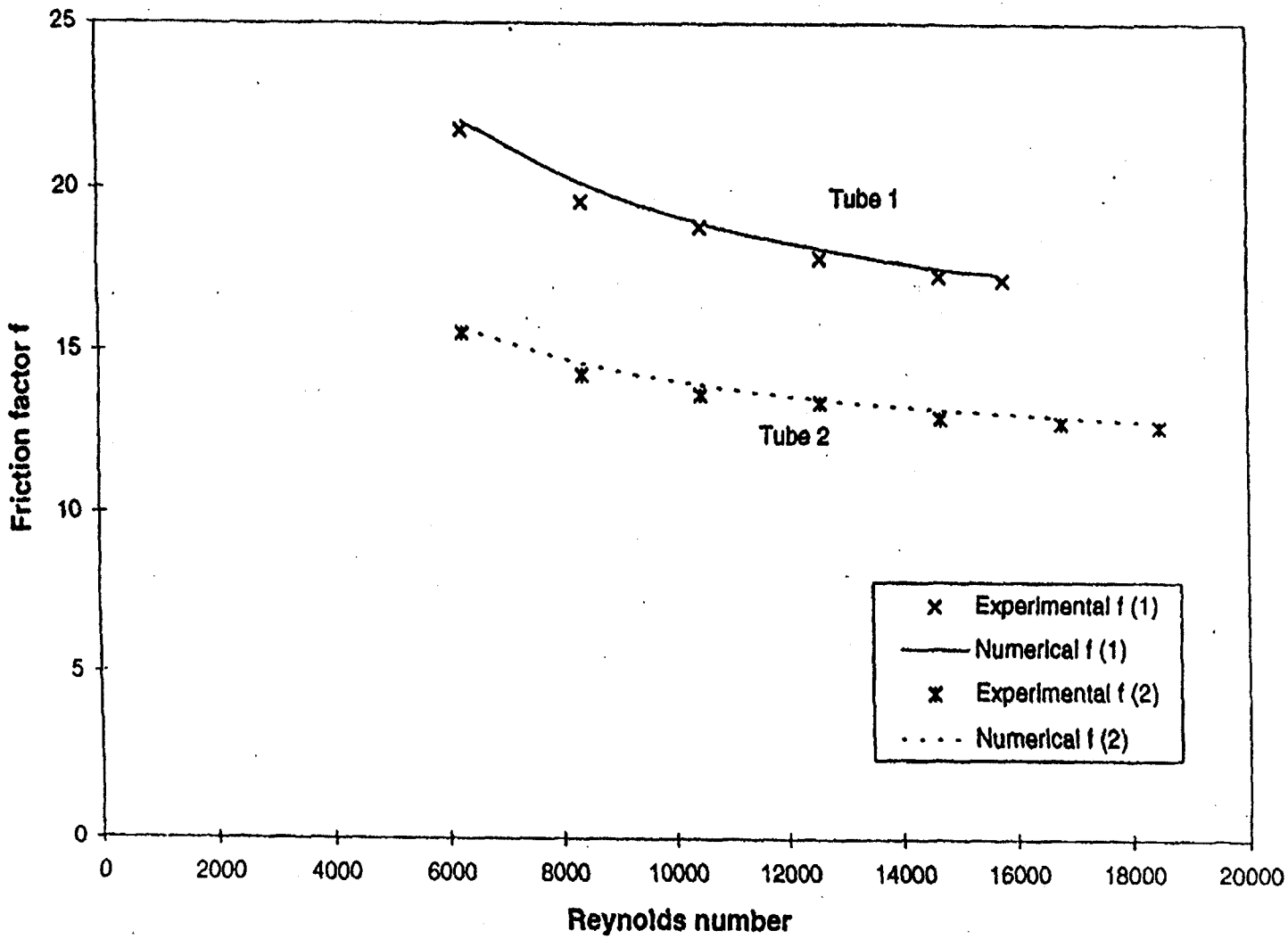
25
20
15
10
5
0
Friction factor f
Tube 1
Tube 2
Experimental f (1)
Numerical f (1)
Experimental f (2)
Numerical f (2)
0
2000
4000
6000
8000
10000
12000
14000
16000
18000
20000
Reynolds number

Fig. 9

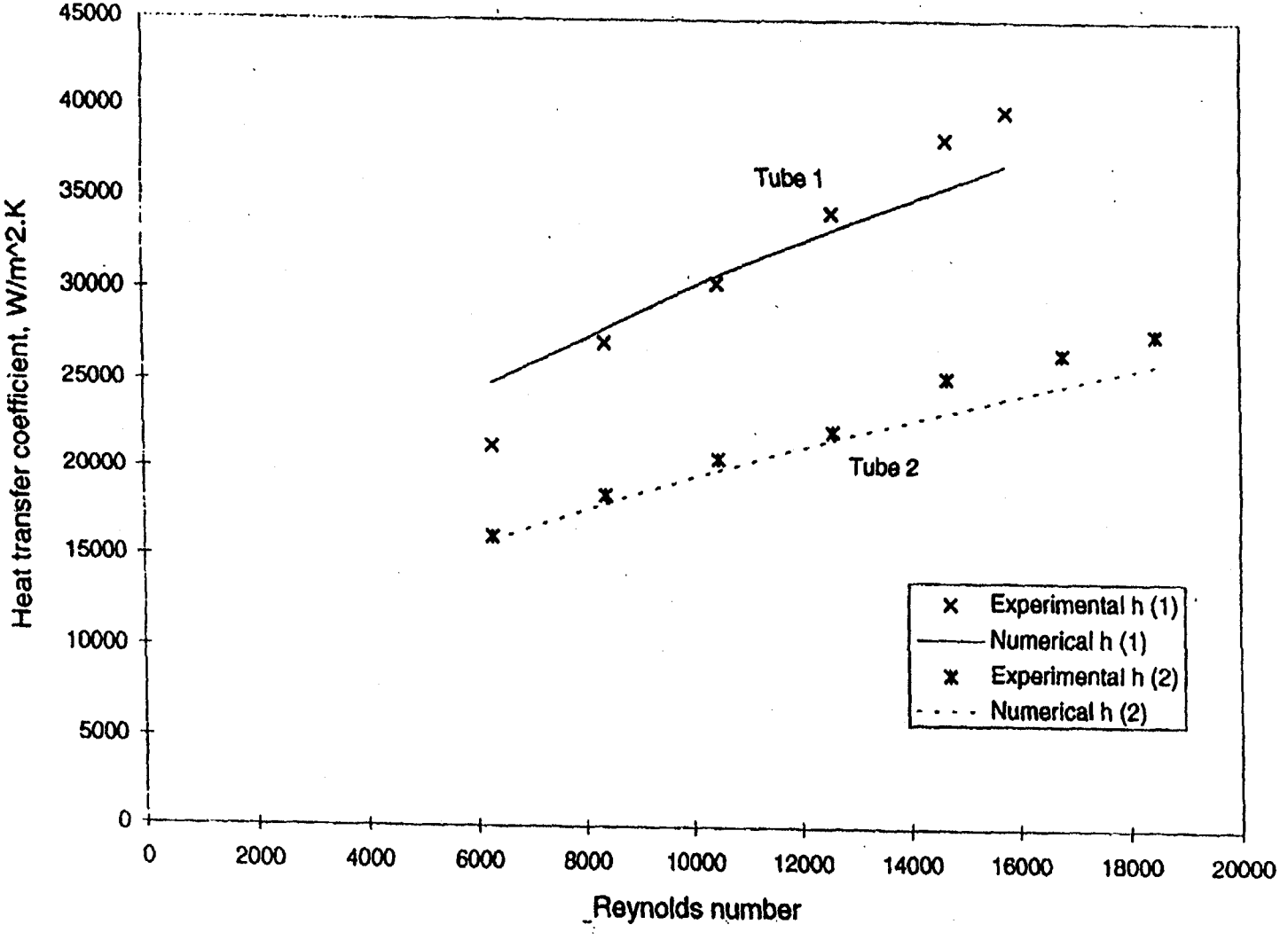
45000
40000
35000
30000
25000
20000
15000
10000
5000
0
Heat transfer coefficient, W/m^2.K
0
2000
4000
6000
8000
10000
12000
14000
16000
18000
20000
Reynolds number
Tube 1
Tube 2
Experimental h (1)
Numerical h (1)
Experimental h (2)
Numerical h (2)

Fig. 10

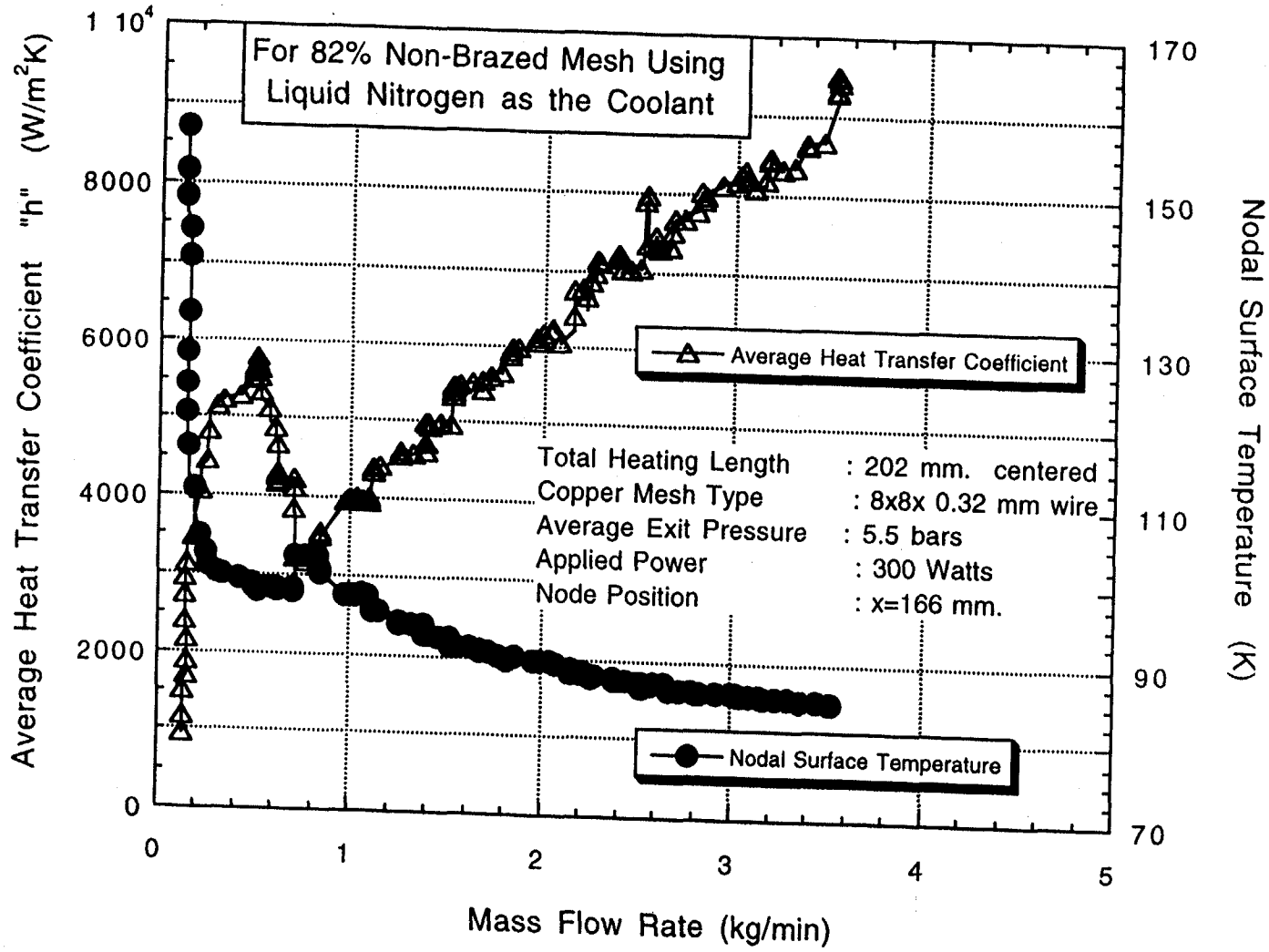
For 82% Non-Brazed Mesh Using
Liquid Nitrogen as the Coolant
Average Heat Transfer Coefficient
Nodal Surface Temperature
Total Heating Length : 202 mm. centered
Copper Mesh Type : 8x8x 0.32 mm wire
Average Exit Pressure : 5.5 bars
Applied Power : 300 Watts
Node Position : x=166 mm.
Average Heat Transfer Coefficient "h" (W/m²K)
1 10⁴
8000
6000
4000
2000
0
Nodal Surface Temperature (K)
170
150
130
110
90
70
0
1
2
3
4
5
Mass Flow Rate (kg/min)

Fig. 11

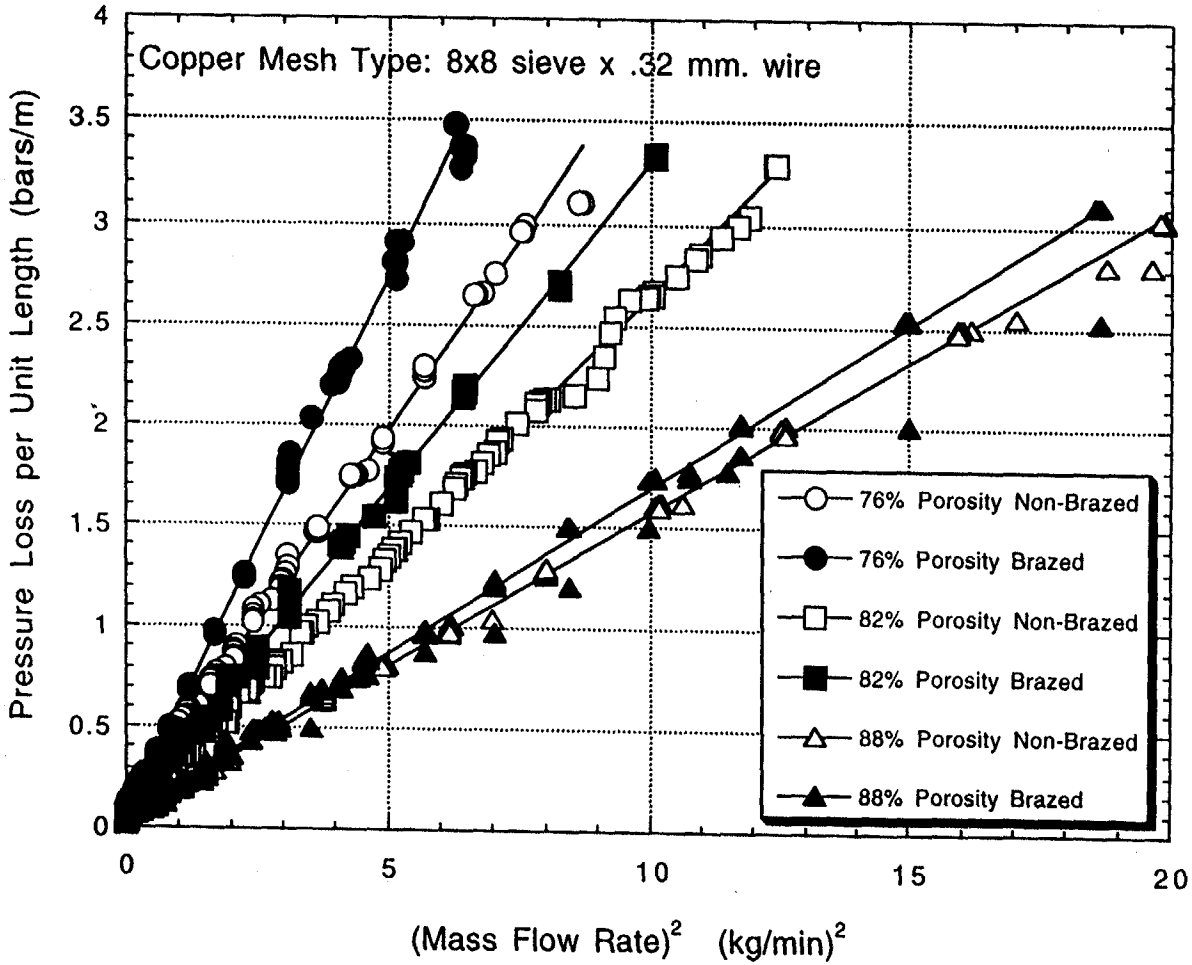
Copper Mesh Type: 8x8 sieve x .32 mm. wire
Pressure Loss per Unit Length (bars/m)
(Mass Flow Rate)^2 (kg/min)^2
0
0.5
1
1.5
2
2.5
3
3.5
4
0
5
10
15
20
76% Porosity Non-Brazed
76% Porosity Brazed
82% Porosity Non-Brazed
82% Porosity Brazed
88% Porosity Non-Brazed
88% Porosity Brazed

Fig. 12

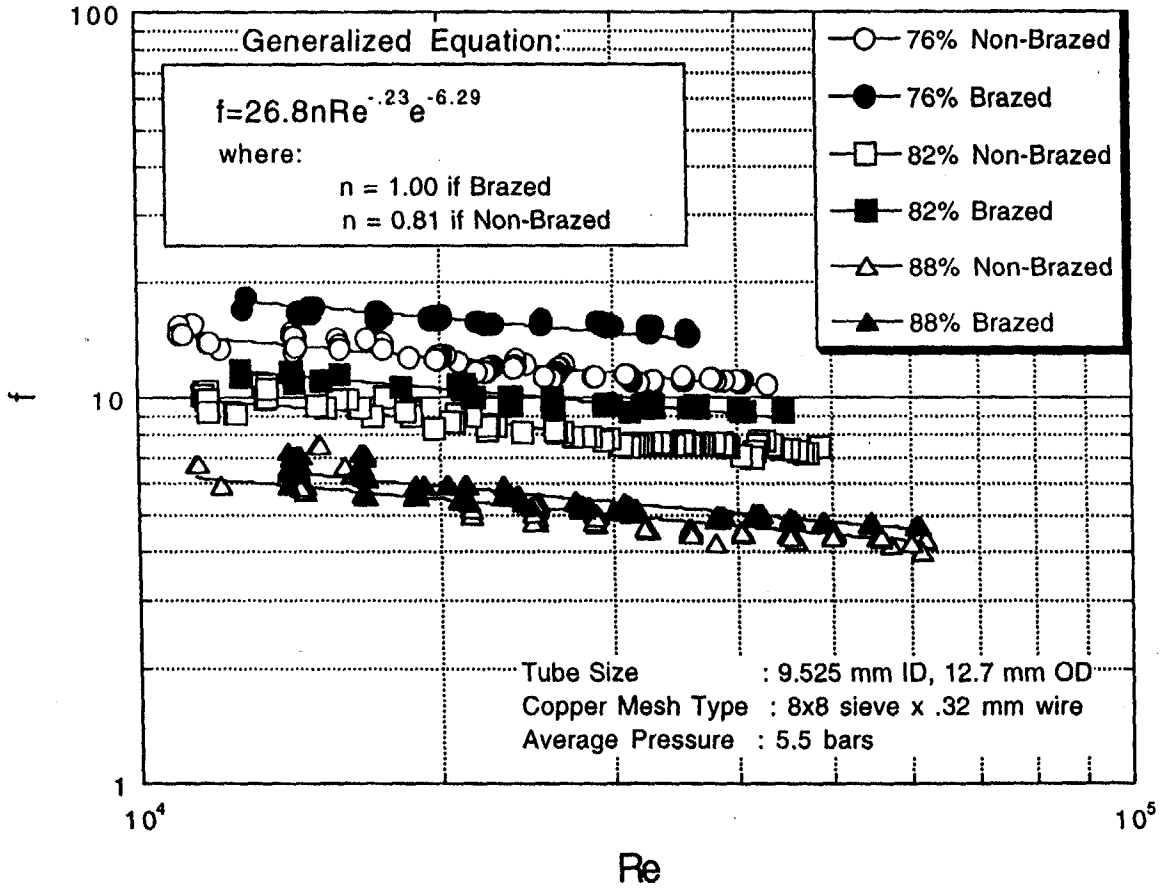
100
10
1
f
Generalized Equation:
f=26.8nRe^-.23 e^-6.29
where:
n = 1.00 if Brazed
n = 0.81 if Non-Brazed
76% Non-Brazed
76% Brazed
82% Non-Brazed
82% Brazed
88% Non-Brazed
88% Brazed
Tube Size : 9.525 mm ID, 12.7 mm OD
Copper Mesh Type : 8x8 sieve x .32 mm wire
Average Pressure : 5.5 bars
10^4
10^5
Re

Fig. 13

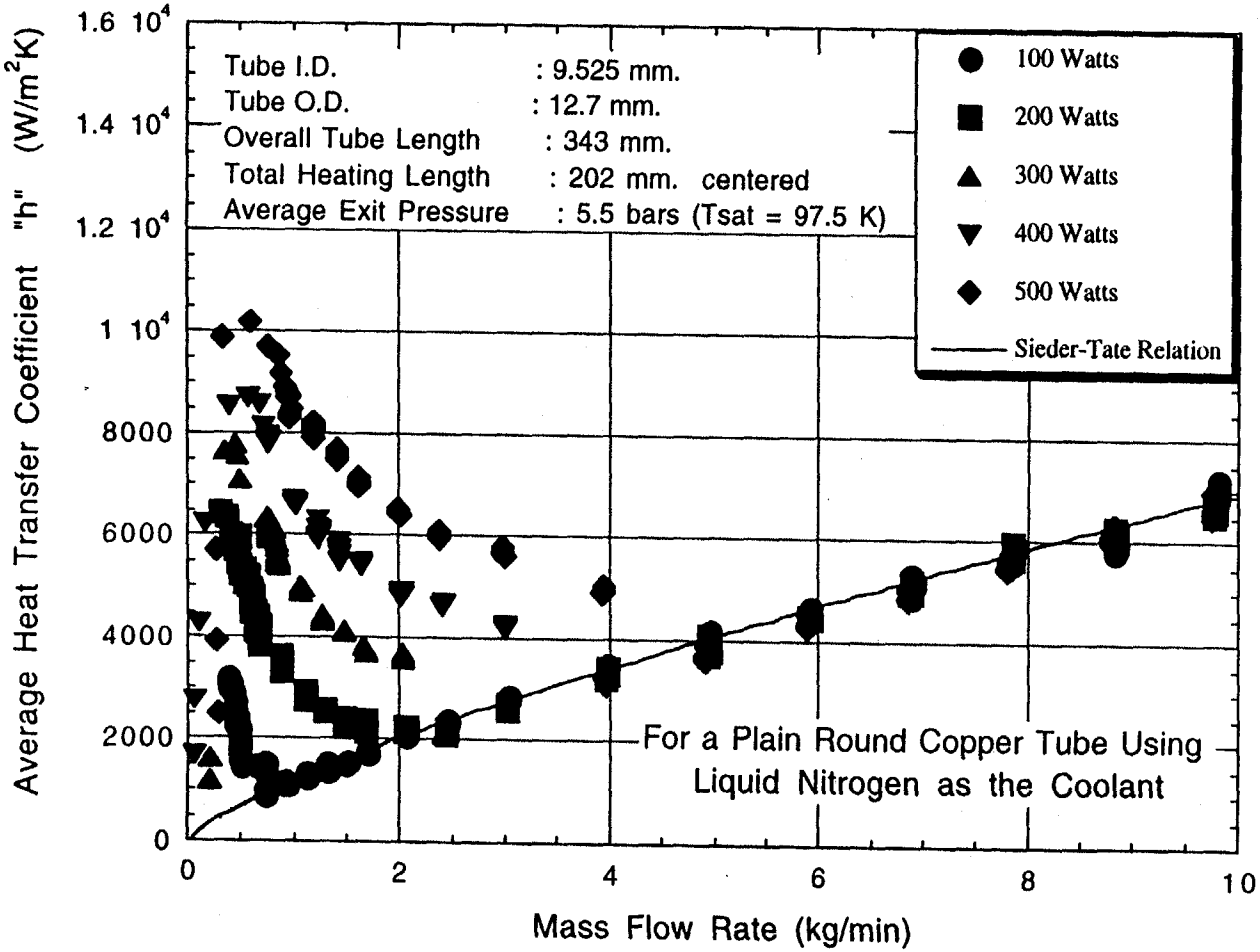
Average Heat Transfer Coefficient "h" (W/m²K)
1.6 10⁴
1.4 10⁴
1.2 10⁴
1 10⁴
8000
6000
4000
2000
0
0
2
4
6
8
10
Mass Flow Rate (kg/min)
Tube I.D. : 9.525 mm.
Tube O.D. : 12.7 mm.
Overall Tube Length : 343 mm.
Total Heating Length : 202 mm. centered
Average Exit Pressure : 5.5 bars (Tsat = 97.5 K)
100 Watts
200 Watts
300 Watts
400 Watts
500 Watts
Sieder-Tate Relation
For a Plain Round Copper Tube Using
Liquid Nitrogen as the Coolant

Fig. 14

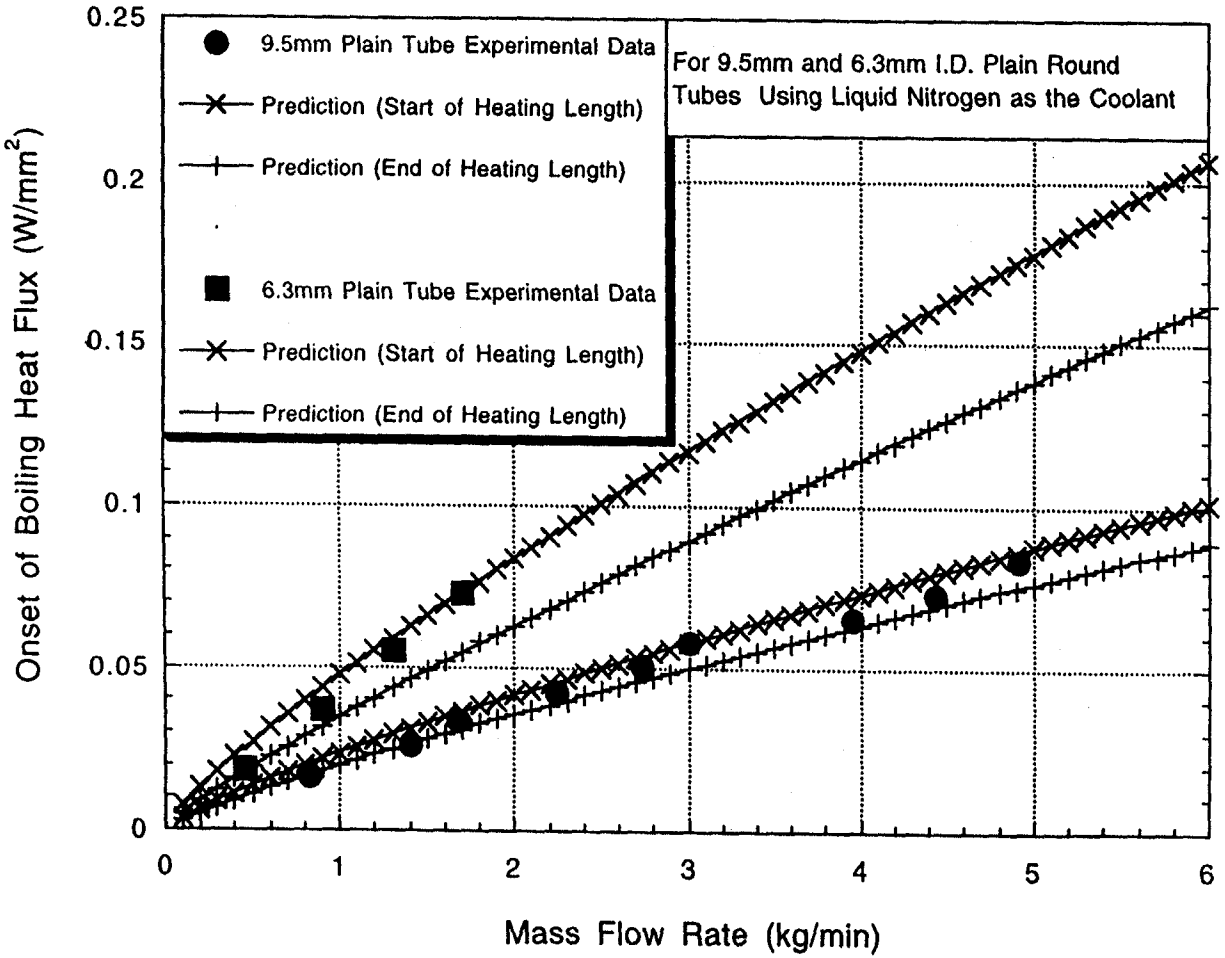
9.5mm Plain Tube Experimental Data
Prediction (Start of Heating Length)
Prediction (End of Heating Length)
6.3mm Plain Tube Experimental Data
Prediction (Start of Heating Length)
Prediction (End of Heating Length)
For 9.5mm and 6.3mm I.D. Plain Round Tubes Using Liquid Nitrogen as the Coolant
Onset of Boiling Heat Flux (W/mm^2)
0.25
0.2
0.15
0.1
0.05
0
0
1
2
3
4
5
6
Mass Flow Rate (kg/min)

Fig. 15

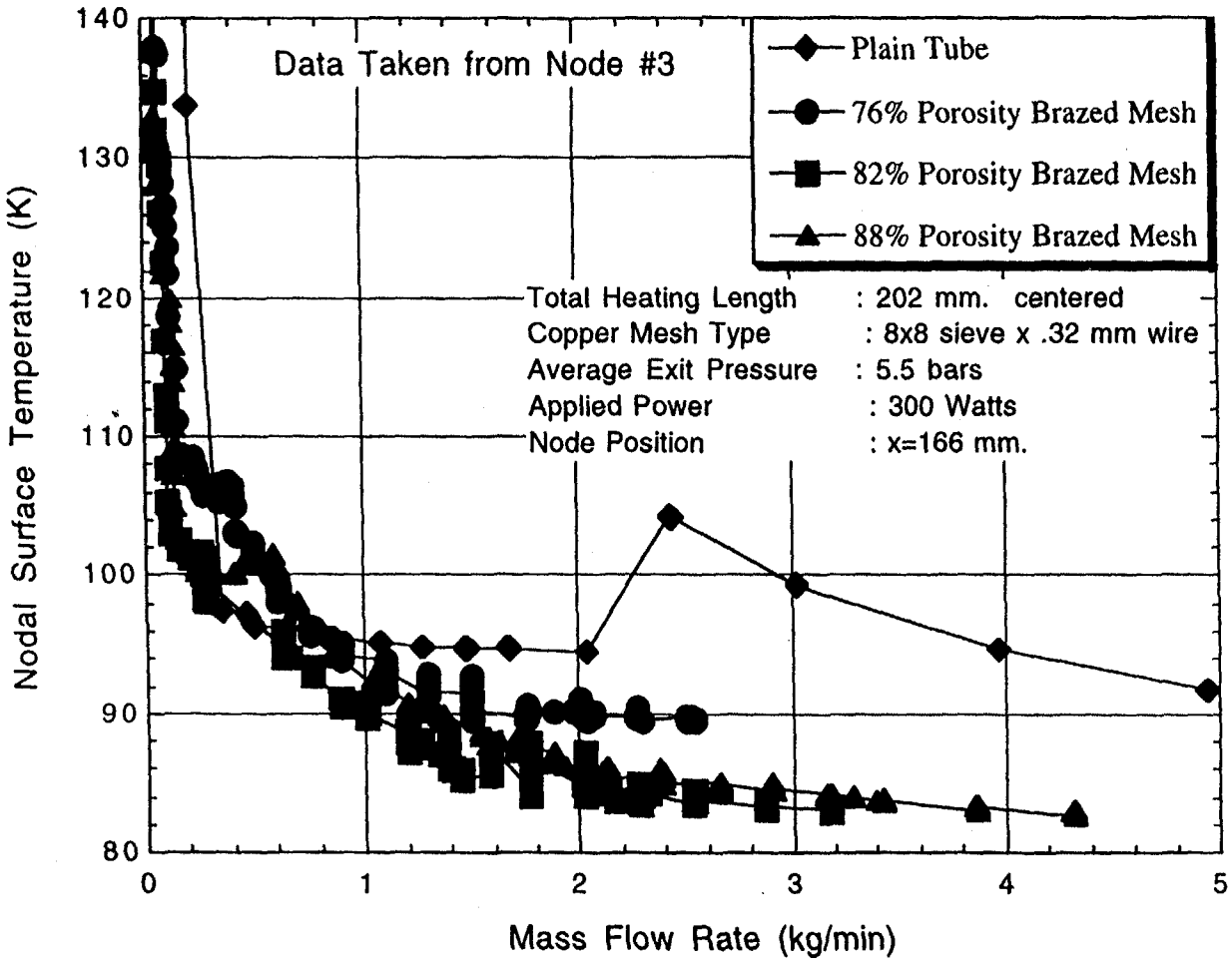
Data Taken from Node #3
Plain Tube
76% Porosity Brazed Mesh
82% Porosity Brazed Mesh
88% Porosity Brazed Mesh
Total Heating Length : 202 mm. centered
Copper Mesh Type : 8x8 sieve x .32 mm wire
Average Exit Pressure : 5.5 bars
Applied Power : 300 Watts
Node Position : x=166 mm.
Nodal Surface Temperature (K)
140
130
120
110
100
90
80
0
1
2
3
4
5
Mass Flow Rate (kg/min)

Fig. 16

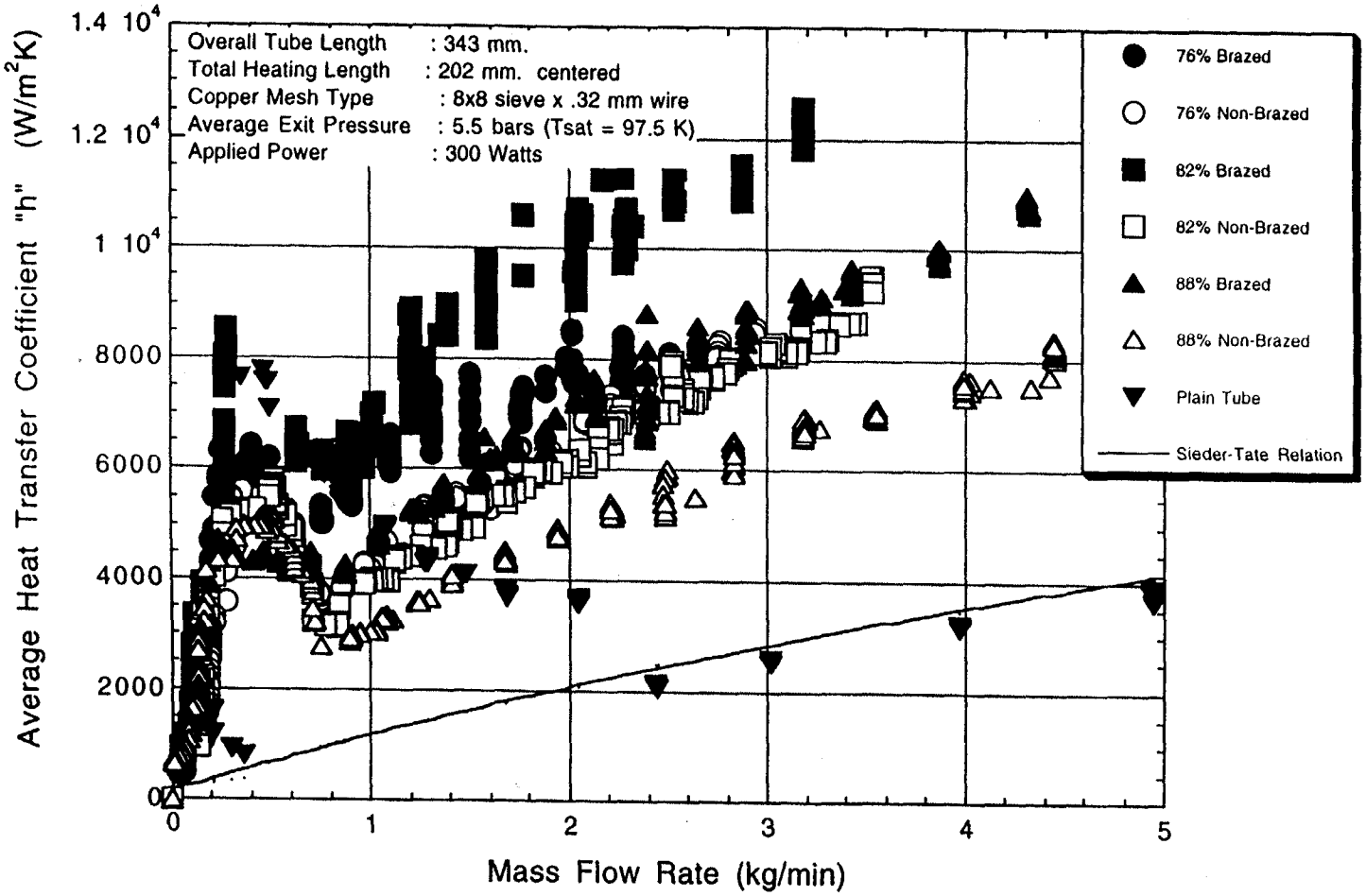
Overall Tube Length : 343 mm.
Total Heating Length : 202 mm. centered
Copper Mesh Type : 8x8 sieve x .32 mm wire
Average Exit Pressure : 5.5 bars (Tsat = 97.5 K)
Applied Power : 300 Watts
76% Brazed
76% Non-Brazed
82% Brazed
82% Non-Brazed
88% Brazed
88% Non-Brazed
Plain Tube
Sieder-Tate Relation
Average Heat Transfer Coefficient "h" (W/m²K)
1.4 10⁴
1.2 10⁴
1 10⁴
8000
6000
4000
2000
0
0
1
2
3
4
5
Mass Flow Rate (kg/min)

Fig. 17

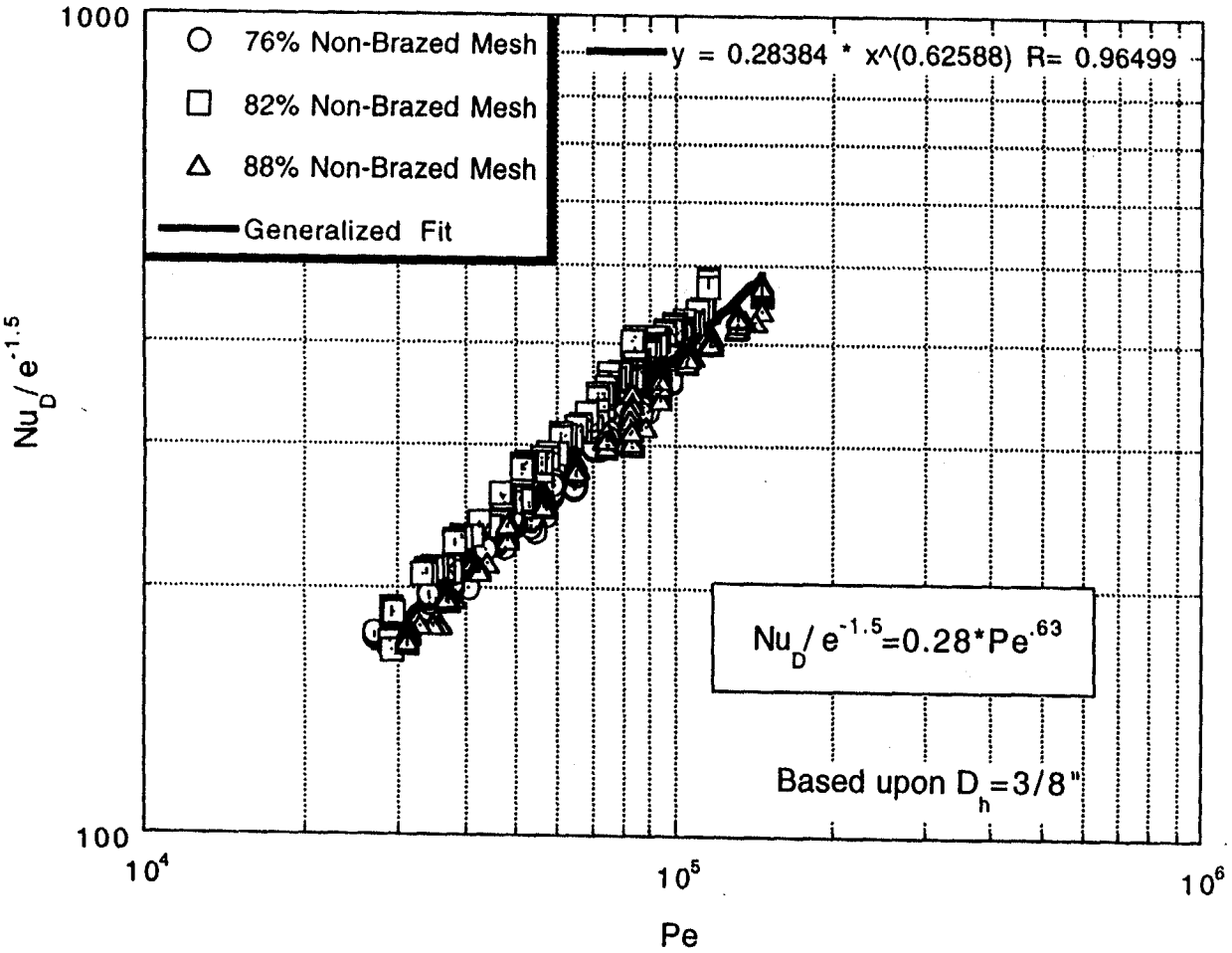
1000
100
10^4
10^5
10^6
Pe
$Nu_D / e^{-1.5}$
76% Non-Brazed Mesh
82% Non-Brazed Mesh
88% Non-Brazed Mesh
Generalized Fit
y = 0.28384 * x^(0.62588) R= 0.96499
$Nu_D / e^{-1.5}=0.28*Pe^{.63}$
Based upon D_h=3/8"

Fig. 18

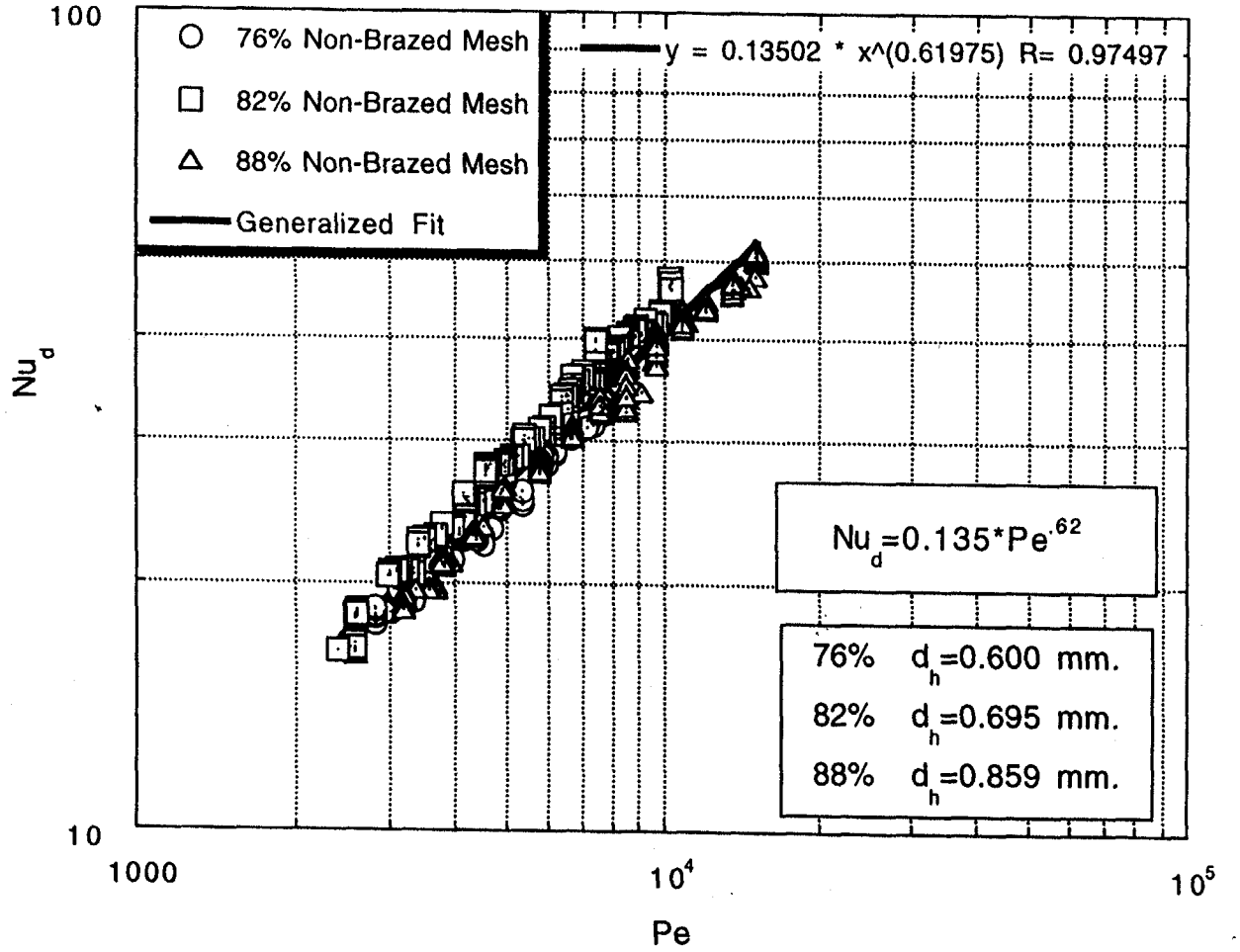
100
10
1000
10^4
10^5
Pe
Nu_d
76% Non-Brazed Mesh
82% Non-Brazed Mesh
88% Non-Brazed Mesh
Generalized Fit
y = 0.13502 * x^(0.61975) R= 0.97497
$Nu_d=0.135*Pe^{.62}$
76% d_h=0.600 mm.
82% d_h=0.695 mm.
88% d_h=0.859 mm.

Fig. 19

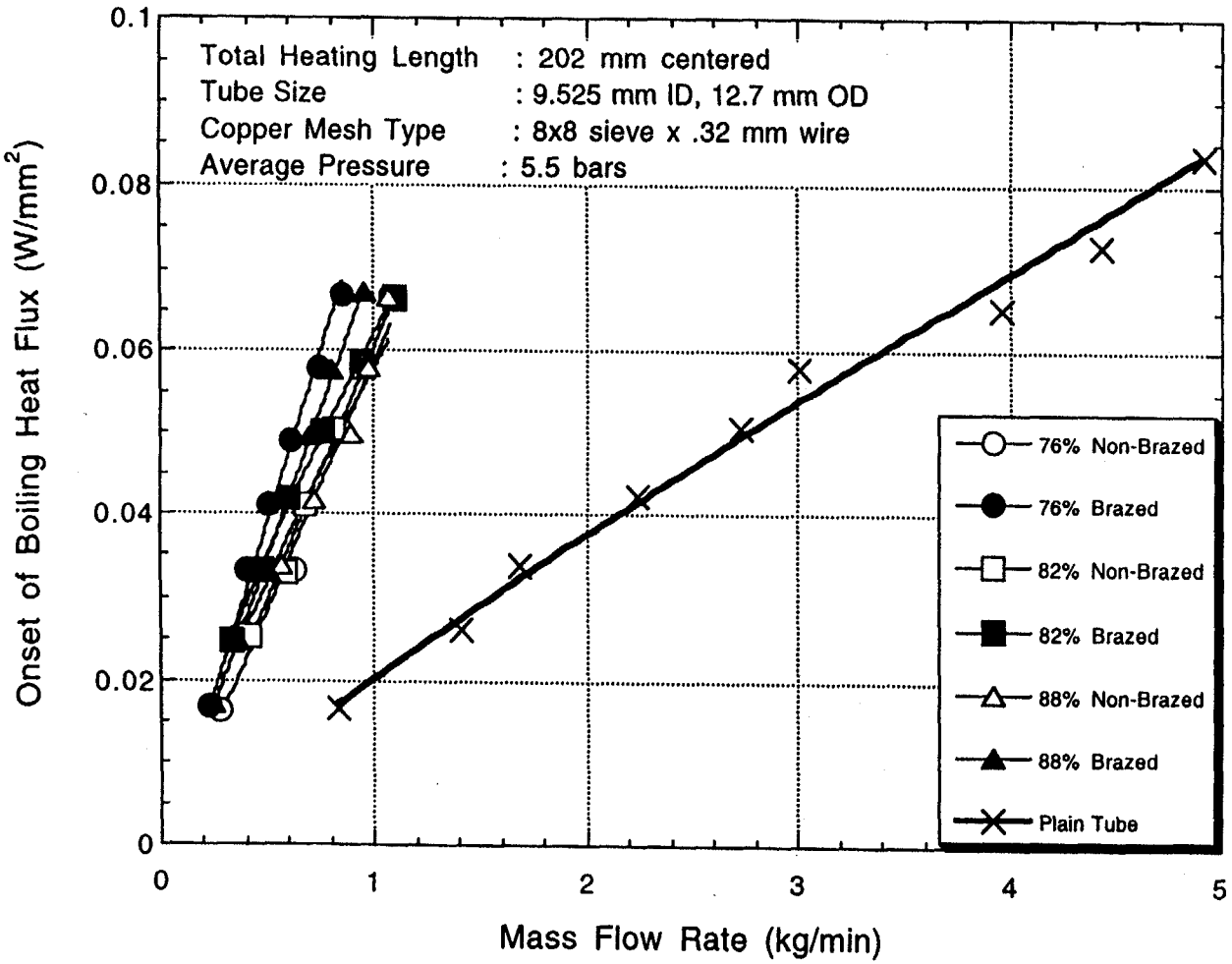
Total Heating Length : 202 mm centered
Tube Size : 9.525 mm ID, 12.7 mm OD
Copper Mesh Type : 8x8 sieve x .32 mm wire
Average Pressure : 5.5 bars
Onset of Boiling Heat Flux (W/mm²)
Mass Flow Rate (kg/min)
0.1
0.08
0.06
0.04
0.02
0
0
1
2
3
4
5
76% Non-Brazed
76% Brazed
82% Non-Brazed
82% Brazed
88% Non-Brazed
88% Brazed
Plain Tube

Fig. 20

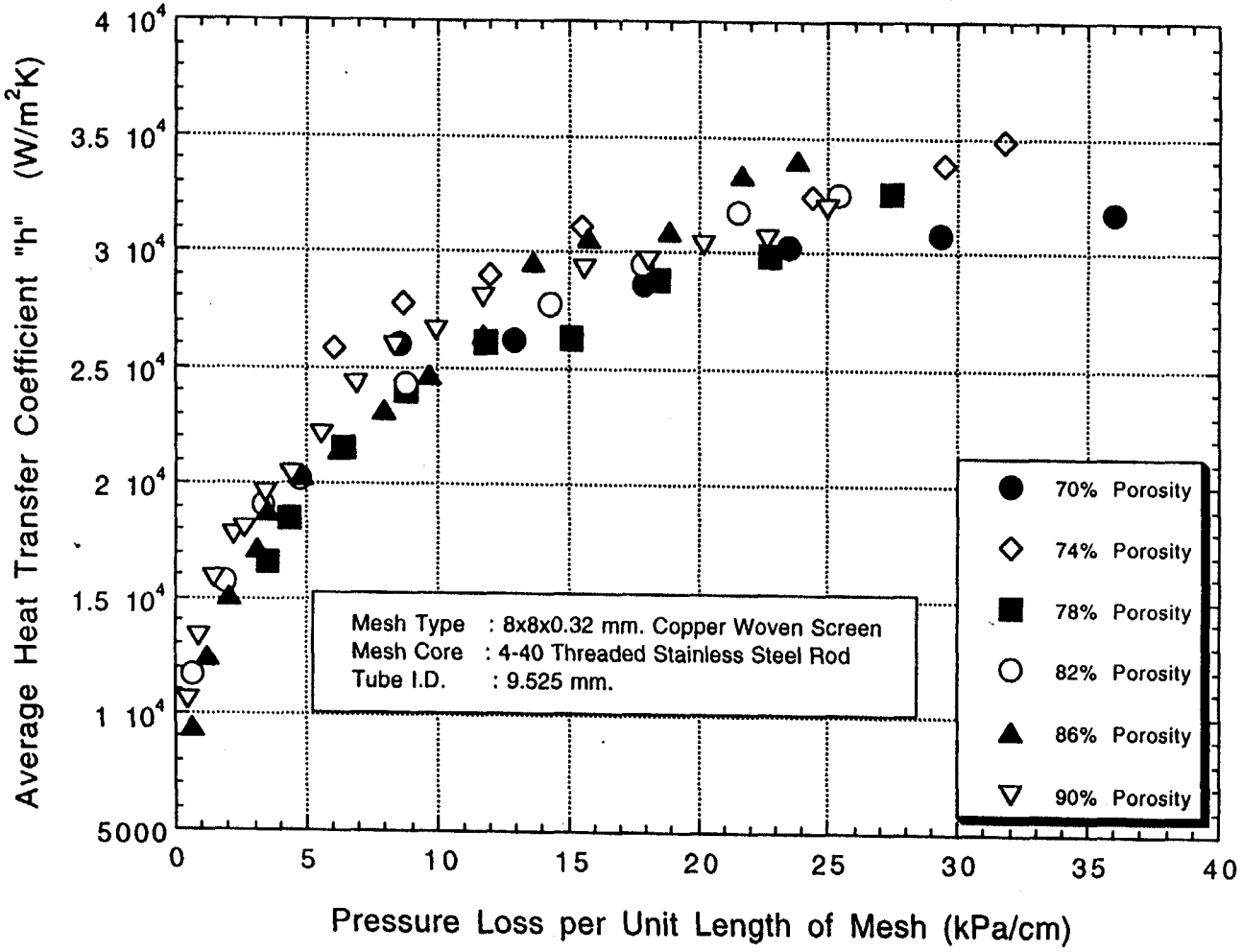
Average Heat Transfer Coefficient "h" (W/m²K)
4 10⁴
3.5 10⁴
3 10⁴
2.5 10⁴
2 10⁴
1.5 10⁴
1 10⁴
5000
0
5
10
15
20
25
30
35
40
Pressure Loss per Unit Length of Mesh (kPa/cm)
Mesh Type : 8x8x0.32 mm. Copper Woven Screen
Mesh Core : 4-40 Threaded Stainless Steel Rod
Tube I.D. : 9.525 mm.
70% Porosity
74% Porosity
78% Porosity
82% Porosity
86% Porosity
90% Porosity

Fig. 21

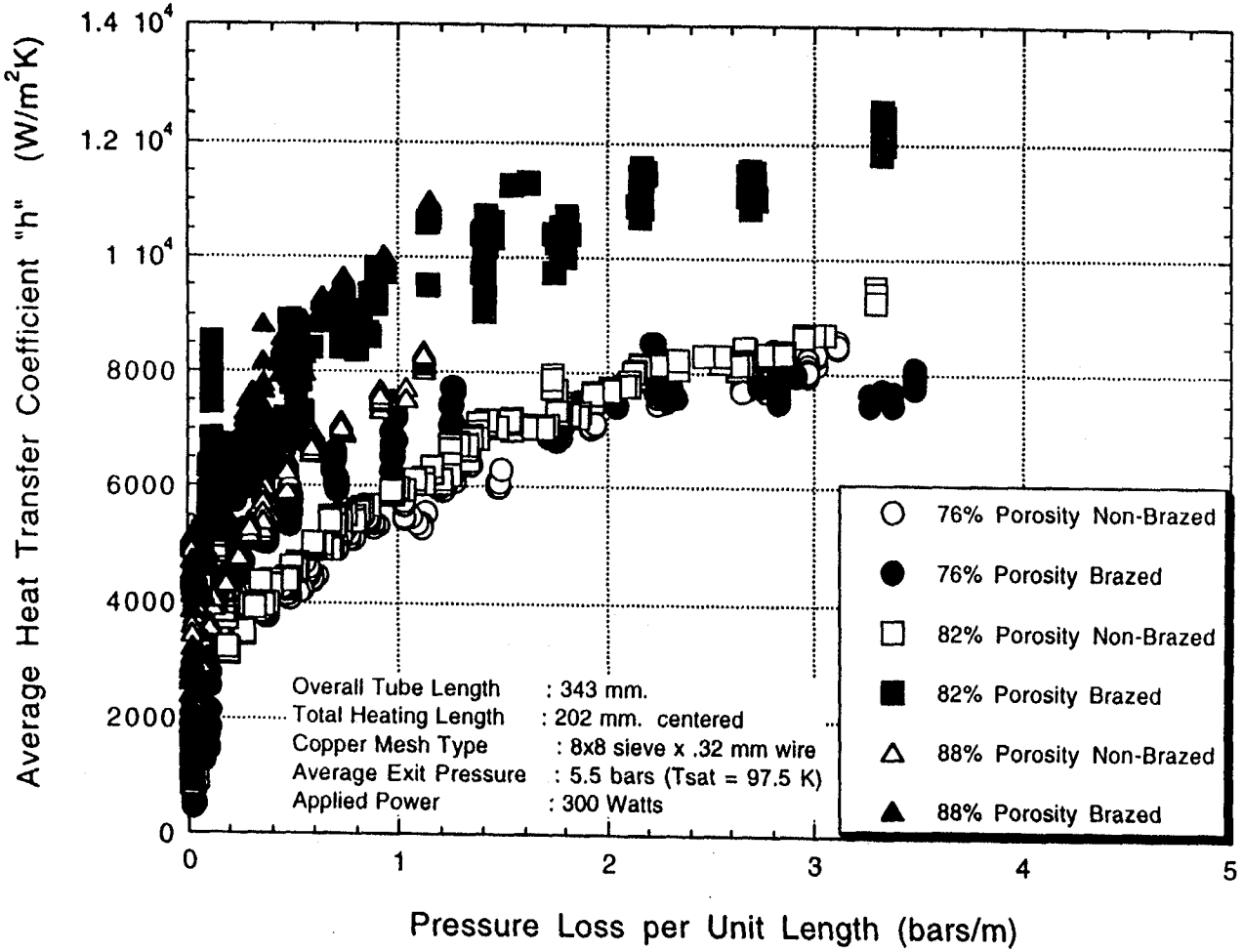
Average Heat Transfer Coefficient "h" (W/m²K)
1.4 10⁴
1.2 10⁴
1 10⁴
8000
6000
4000
2000
0
0
1
2
3
4
5
Pressure Loss per Unit Length (bars/m)
Overall Tube Length : 343 mm.
Total Heating Length : 202 mm. centered
Copper Mesh Type : 8x8 sieve x .32 mm wire
Average Exit Pressure : 5.5 bars (Tsat = 97.5 K)
Applied Power : 300 Watts
76% Porosity Non-Brazed
76% Porosity Brazed
82% Porosity Non-Brazed
82% Porosity Brazed
88% Porosity Non-Brazed
88% Porosity Brazed

Fig. 22